ELASTIC RECOVERY OF IMMISCIBLE POLYMER BLENDS

by

Jun Wang

B.S. in ChE., East China University of Science and Technology, 1996

M.S. in ChE., East China University of Science and Technology, 1999

Submitted to the Graduate Faculty of

School of Engineering in partial fulfillment

of the requirements for the degree of

Master of Science in Chemical Engineering

University of Pittsburgh

2004

UNIVERSITY OF PITTSBURGH

SCHOOL OF ENGINEERING

This thesis was presented

by

Jun Wang

It was defended on

October 14, 2004

and approved by

Joseph J. McCarthy, Associate Professor, Chemical and Petroleum Engineering Department, University of Pittsburgh

Lynn M. Walker, Associate Professor, Chemical Engineering Department, Carnegie Mellon University

Thesis Advisor:
Sachin Velankar, Assistant Professor, Chemical and Petroleum Engineering Department, University of Pittsburgh

ABSTRACT

ELASTIC RECOVERY OF IMMISCIBLE POLYMER BLENDS

Jun Wang, M.S.

University of Pittsburgh, 2004

Interfacially active species, called compatibilizers, are often added when blending immiscible polymers to promote blending and improve product properties. The effects of compatibilizer on the rheological properties of polymer blends are considered here.

Blends of immiscible Polyisobutylene (PIB) and Polydimethyl siloxane (PDMS) compatibilized by a diblock copolymer of PIB and PDMS were studied. Blends had droplet matrix morphologies contained up to 30 wt. % of PIB and up to 1 wt. % of compatibilizer. The ratio of viscosity of the PIB to that of the PDMS was varied from 0.29 to 1.7.

In blends without compatibilizer, the recovery was a single-retardation time process. The ultimate recovery and retardation time were found to increase with wt. fraction of the dispersed phase and with the capillary number; and decrease with increasing viscosity ratio. A previously developed model by Vinckier *et al.* was found to predict the retardation time well, but overpredicted the ultimate recovery.

In blends with compatibilizer, recovery was no longer a single retardation time process. Compatibilizer was found to increase ultimate recovery and retardation time under all conditions studied. The largest increase occurred at the lowest viscosity ratio. Moreover, under certain flow conditions, a weak but very slow recovery process was observed. The results may be explained by a coupling between flow and compatibilizer concentration on the interface, however, the phenomena are too complex to draw a firm conclusion based on the available data.

DESCRIPTORS

Compatibilizer

Creep recovery

Immiscible Polymer Blends

Interfacial tension

Surfactant

Viscoelasticity

.

TABLE OF CONTENTS

LIST OF TABLES

LIST OF FIGURES

ACKNOWLEDGEMENT

I would like to gratefully acknowledge my advisor Professor Sachin Velankar for his patience and great guidance during this study. His encouragement and generosity allowed me to accomplish this work. My gratitude to him can't be expressed in words.

I am grateful to the Lab of Applied Rheology at the K.U. Leuven, Belgium for making the block copolymer available for this research.

I also thank my colleagues, Prachi, Jeffrey, and Todd. We have a good time to work together.

I dedicate this thesis to my Mother. I am grateful to her for always encouraging me to pursue the knowledge in new areas and for her unfailing support and love.

1. 0 INTRODUCTION

Blending of immiscible polymers provides an economic alternative to synthesizing new polymers. The trend is to use well-known components and to blend them in the melt to achieve the required properties. Instead of synthesizing new materials, blending is preferred as a faster, easier and cheaper way of developing new materials. The polymers being blended are often immiscible, and various morphologies may occur during blending. For example, polystyrene which is a brittle material, and polybutadiene which is rubbery, are immiscible. The immiscible blends of these two polymers have high fracture toughness and flexibility and are sold commercially under the name high-impact polystyrene (HIPS).

Properties of immiscible polymer blends are known to depend strongly on the detailed morphology [1]. Droplets/matrix, fibrillar, lamellar or co-continuous morphologies have been observed [2]. During processing, flow can cause drastic changes in the microstructure of two-phase fluids. The resulting morphology depends on several factors such as composition, processing conditions (mixing time, temperature, shear or elongational rate) or nature of the polymers (interfacial tension, viscosity, elasticity) [2]. The evolution of the microstructure in fluid-fluid systems has been the subject of many theoretical and experimental studies.

1.1 PROBLEM DESCRIPTION

Most research has focused on droplets/matrix morphologies. The understanding of the behavior of a liquid drop suspended in a liquid continuous phase is of major significance to such morphologies.

The first stage in understanding the action of emulsification was to consider the deformation and break-up of droplets in the surrounding continuous phase. Taylor's work was probably the first quantitative analysis of the mechanics of the blending process of two immiscible fluids to be published [3-5]. Previous studies by Rayleigh [6, 7], had simply concentrated on the effect of surface tension in causing instability and droplet break-up. The Taylor analysis was the first to consider the distortion of a droplet caused by the viscous stresses exerted by the surrounding continuous phase [5].

Consider a drop of Newtonian fluid of viscosity η_d suspended in an unbounded Newtonian fluid of viscosity η_m (Fig.1.1). The undeformed radius of the drop is denoted by R and the interfacial tension acting between the two fluid phases is denoted by σ. The capillary number, Ca, represents the ratio of viscous forces to surface tension, where

$$Ca = \frac{\eta \dot{\gamma} R}{\sigma} \tag{1-1}$$

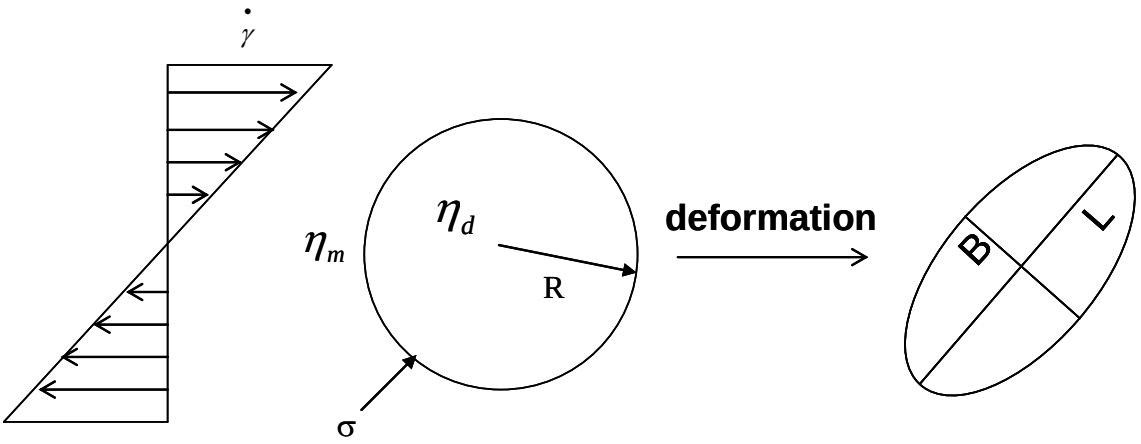

Fig.1.1 Schematic of drop deformation in shear flow

1.1.1 Drop Deformation

When a neutrally buoyant drop is placed in a shear flow, it will deform. For all viscosity ratios, the drop shape will be nearly spherical provided the capillary number (Ca) is sufficiently small. In this limit a small deformation analysis is valid and predicts the drop deformation D(Ca), and its orientation in the flow [3, 4].

When Ca<< 1, the deformation, D, is linear in Ca, as first demonstrated by Taylor [4], and

$$D = \frac{L+B}{L-B} = \frac{(19p+16)Ca}{16p+16} \tag{1-2}$$

where L and B are shown in Fig. 1.1, and p is the ratio of the drop viscosity to the matrix viscosity,

$$p = \frac{\eta_d}{\eta_m} \tag{1-3}$$

A drop will maintain a nearly spherical shape at all Ca in shear flow provided p >> 1. On the other hand, for low viscosity ratios, p <<1, the application of a sufficiently large shear rate (Ca>>1) forms steady, highly elongated slender drop shapes with nearly pointed ends.

1.1.2 Drop Breakup Under Shear Flow

As the capillary number is increased the drop becomes increasingly elongated. There is a critical condition beyond which no steady drop shape exists. The critical capillary number for breakup, Ca_c, corresponds to the smallest steady rate $\dot{\gamma}$ for which the drop is unable to maintain a steady shape, and therefore undergoes a transient, continuous stretching. When the critical capillary number is exceeded, drop stretches and thins, eventually breaking up (Fig.1.2). If the drop radius becomes sufficiently small before breakup, capillary waves can cause the highly elongated drop to fragment during flow, though this response requires very large elongations, typically greater than 20 times the initial drop radius [8].

1.1.3 Drop Breakup Under Quiescent Conditions

If the flow is stopped once the drop is deformed, the subsequent changes in drop shape depend on the deformation. If the drop was stretched below D_c (some critical value of deformation), the deformed drop will recover back to a spherical shape, shown as Fig.1.3. If the drop was stretched beyond D_c, the drop starts recovering back towards spherical shape, then subsequently

fragments, forming a number of smaller drops. If the deformation is modest, breakup occurs by "end-pinching" which was observed previously in the experiments of Taylor [4] and Grace [9] (Fig 1.4). End-pinching is a consequence of an interfacial-tension-driven flow associated with curvature variations along the surface of the finite drop. The drop attempts to return to a spherical shape, though fluid motions produced by internal pressure gradients lead to break up. If the deformation is very large, breakup occurs by capillary instability [10-13][Fig.1.5].

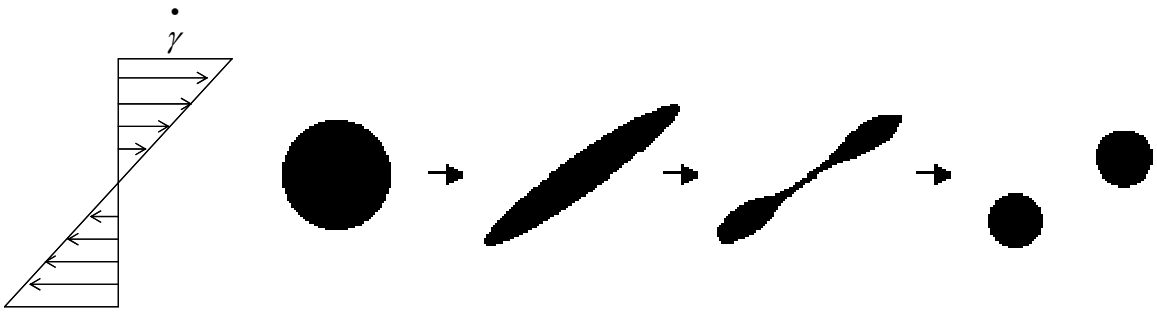

Fig.1.2 Schematic of drop breakup in shear flow

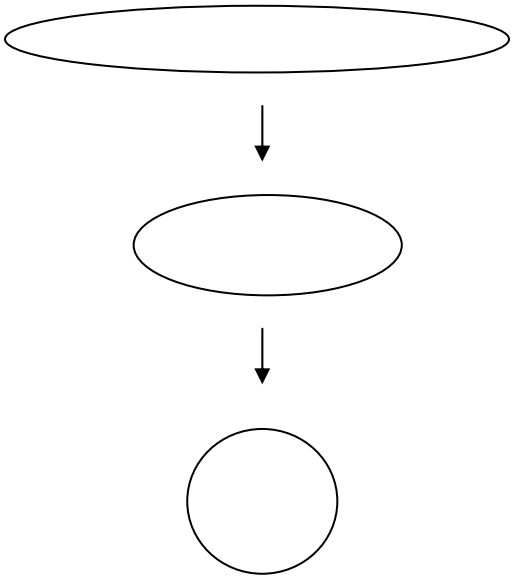

Fig.1.3 Schematic of drop recovery after cessation of shear flow

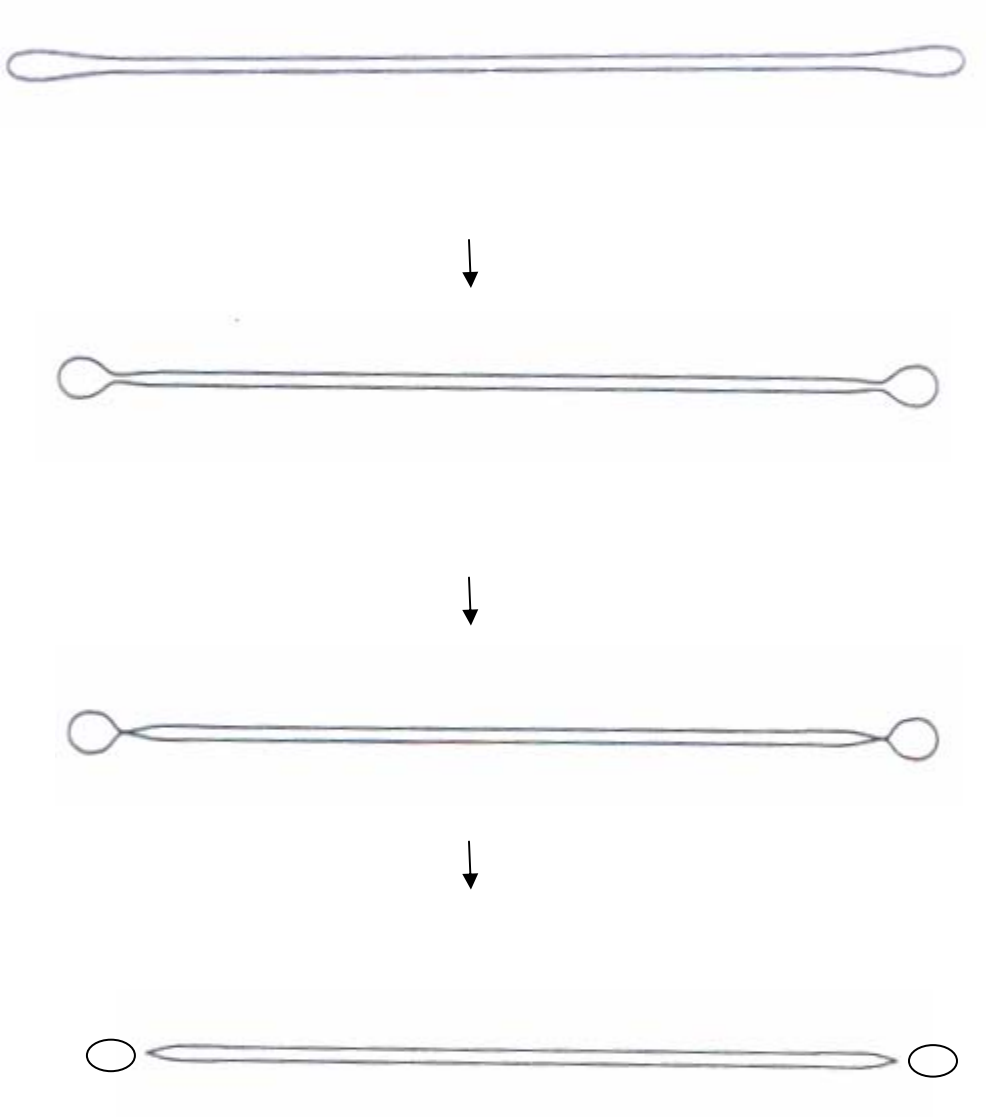

Fig.1.4 Schematic of end-pinching under quiescent conditions. Reprinted with permission from Stone, H.A. [14, 15]

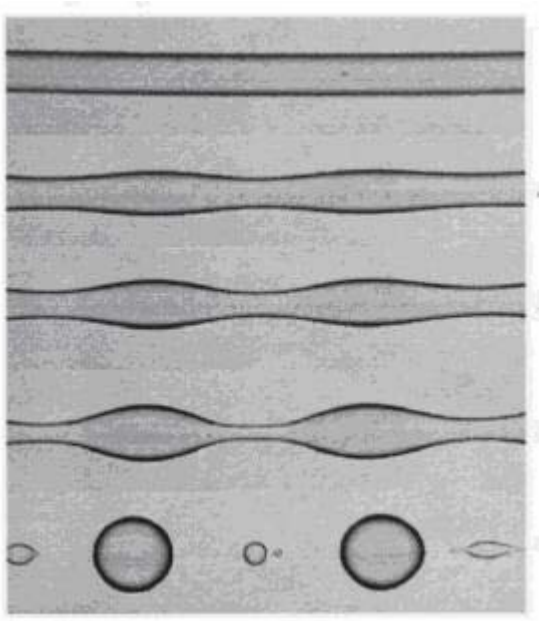

Fig.1.5 Capillary-wave instability under quiescent conditions. Reprinted with permission from Son, Y et al. [16]

1.2 RHEOLOGY OF IMMISCIBLE BLENDS

Immiscible blends combine characteristics of both constituent polymers in a manner that depends strongly on the microstructure of the blend, as it is generated during the processing. In order to optimize the final structure of blends, good insight into the relationship between the blend morphology and its rheological behavior is essential. There are two aspects to this relationship: the applied flow history can change the blend morphology, and the two-phase morphology affects the rheology. We will first consider the viscosity of droplet-matrix morphologies, and then discuss more complex rheological properties.

1.2.1 Zero Shear Viscosity

The simplest case to consider is steady flow of a dilute emulsion of Newtonian drops in Newtonian medium. If the capillary number is small, so that the drops deform only slightly under flow, then at steady state the viscosity of the emulsion is given by Taylor's extension of the Einstein formula for solid spheres [3]:

$$\frac{\eta}{\eta_m} = 1 + \frac{1 + 2.5p}{1 + p}\phi \tag{1-4}$$

where, η is the viscosity of the emulsion, η_m is the viscosity of the matrix, and p is the ratio of the viscosities of the dispersed to the suspending fluids. In the limit of a very viscous droplet fluid, p→ ∞, the droplets behave like hard spheres, and Einstein's results, $\frac{\eta}{\eta_m} = 1 + 2.5\phi$, is recovered. In the opposite limit, p→ 0 (which is usually valid for bubbles), the relative viscosity is lower, $\frac{\eta}{\eta_m} = 1 + \phi$. The viscosity of a suspension of bubbles is less than that of a suspension of hard spheres at a given volume fraction ϕ.

For high concentrations, outside of the dilute regime, Pal [17] has proposed an empirical equation for the zero-shear viscosity of an emulsion:

$$[\frac{\eta}{\eta_m}]^{1/K_1} = \exp[\frac{2.5\phi}{1 - \phi/\phi_m}] \tag{1-5}$$

where

$$K_I = \exp[\frac{0.4 + p}{1 + p}] \tag{1-6}$$

For semi-dilute emulsions, a model has been proposed by Choi and Schowalter[18]. In their expressions for the viscosity, the internal circulation inside the dispersed phase, the droplet deformability and a limited degree of hydrodynamic interactions between the drops is included. When assuming that both components of the emulsion are Newtonian, i.e. having a constant viscosity and no elasticity, and omitting higher order terms in concentration and droplet deformation, Choi and Schowalter obtained the following equations for the emulsion viscosity η[19]:

$$\frac{\eta}{\eta_m} = 1 + \phi \frac{(5p + 2)}{2(p + 1)} \cdot [1 + \phi \frac{5(5p + 2)}{4(p + 1)}] \tag{1-7}$$

1.2.2 Non-Newtonian Behavior

1.2.2.1 Linear Viscoelasticity: Dynamic oscillatory behavior

Much of the experimental work on viscoelasticity of blends focuses on the response of two-phase polymeric mixtures to linear oscillatory flow [20-25]. The most striking result of these experiments is the emergence of a pronounced elasticity at low frequencies due to the interfacial tension. This elasticity arises because deformed droplets relax back to a spherical shape under the influence of interfacial tension. Dimensional analysis suggests that the characteristic time constant for relaxation is proportional to $\frac{R\eta_m}{\sigma}$.

This elastic behavior is most easily probed by measuring the complex modulus

$$G^*(\omega) = G'(\omega) + iG''(\omega) \tag{1-8}$$

in small-amplitude oscillatory shear flow. Using a small strain ensures that the droplets remain nearly spherical and that the stress response is linear in strain. The small strain also ensures that droplet breakup can not happen during the experiments. Moreover, at low volume fraction of drops, quiescent coalescence is slow. Thus, oscillatory shear offers a way to probe the properties of a blend without altering its microstructure.

The main effect of the dispersed phase is to increase the storage modulus G′ at low frequencies. An example of such behavior is shown in Fig. A-1 in Appendix A. The critical frequency of this effect is governed by the relaxation time of droplets. The presence of the droplets has only a small effect on the loss modulus G″.

The first theory of viscoelastic behavior imparted by interfacial tension was developed by Oldroyd [26] for Newtonian phases of nearly spherical droplets. Oldroyd's theory was extended to linear viscoelastic phases by Palierne [27] and Graebling & Muller [22]. Palierne provides a detailed derivation, which includes a distribution of droplets sizes as well as variations in interfacial tension. Although Palierne's theory can be written for a distribution of droplet sizes, for most cases it is sufficient to use the volume-average droplet radius R_v (Graebling *et al.* [21]). Then the complex modulus G* of the blend is given by

$$\frac{G^*(\omega)}{G_m^*(\omega)} = \frac{1+3\phi H(\omega)}{1-2\phi H(\omega)} \tag{1-9}$$

where

$$H(\omega) = \frac{4(\sigma/R_v)(5G_d^* + 2G_m^*) + (G_d^* - G_m^*)(19G_d^* + 16G_m^*)}{40(\sigma/R_v)(G_d^* + G_m^*) + (2G_d^* + 3G_m^*)(19G_d^* + 16G_m^*)} \tag{1-10}$$

For a blend of Newtonian components, the droplet relaxation time τ_D is given by the Palierne theory as

$$\tau_D = \frac{R_v\eta_m}{4\sigma}\frac{(19p+16)(2p+3-2\phi(p-1))}{10(p+1)-2\phi(5p+2)} \tag{1-11}$$

The Palierne theory shows excellent agreement with experiments on a variety of systems [21, 22]. If the droplet size is known, then interfacial tension can be determined by fitting Palierne's theory to experimental curves of $G'(\omega)$ [21, 22] or to relaxation spectra [23].Alternately, if interfacial tension is known, then the low-frequency elastic response can be used to determine the volume-average drop radius R_v. Vinckier *et al.* [28] reported that drop sizes found this way are in good agreement with microscopy data, and they compare several methods of data reduction to find R_v. It may also possible to extract a complete drop-size distribution from rheological data [25]. Measuring the linear viscoelastic spectrum of an immiscible blend has become an established tool for determining the morphology of droplet-matrix blends.

1.2.2.2 Other Non-Newtonian Effects

Other than the increase in G′ at low frequencies, blends also show other non-Newtonian effects such shear thinning, relaxation behavior, normal stress difference, etc.

Blends exhibit shear thinning behavior at low shear rates, even when the components are nearly Newtonian[19, 29]. Shear thinning occurs due to increasing orientation of drops along the flow direction at increasing shear rates. This effect has been captured by the Choi-Schowalter theory, at least qualitatively [18].

After cessation of a steady flow, or after applying a step strain, the deformed droplets shapes are not stable. Driven by interfacial tension, droplets either retract back to spheres or break up into smaller fragments as discussed in Section 1.1.3. This microstructural relaxation is accompanied by stress relaxation. As discussed in Section 1.1.3, microstructural relaxation occurs by one of several mechanisms (retraction without breakup, breakup by a capillary-wave instability, breakup by end pinching), depending on the initial deformation of the droplet and the viscosity ratio [14,15]. Rheological methods are a powerful means of studying such microstructural relaxation since concentrated blends ($\phi > 0.05$) can only be probed through rheological measurements[30]. Other techniques such as optical or rheological methods work only for dilute blends[31-33]. Rheological measurements can discriminate between the different relaxation mechanisms based on the shape of the stress relaxation curves[30].

Deformation and orientation of the interface also results in a normal stress in steady shear flows. This normal stress depends not only on the flow conditions and the material properties, but also on the morphology of the system. The experimental data on droplet-matrix morphologies indicate that the normal stress contribution of the interface is well described by the Choi-Schowalter equation over a wide range of viscosity ratios [19]. The normal stress also displays complex transients which can be explained in terms of the changing microstructure of the blends. It has been demonstrated that the transient rheological response can be used to probe the droplet deformation and break-up in immiscible blends both during flow and during relaxation after cessation of flow [34] .

1.2.2.3 Elastic Recovery of Immiscible Blends

Most of the experimental research in this thesis concerns the recovery of immiscible blends and hence it is described separately in this section. After cessation of a steady flow, or after applying a step strain, the deformed droplet shapes are not stable. Driven by interfacial tension, droplets either retract back to spheres or break up into smaller fragments. This drives strain recovery of the blends [35].

The elastic recovery of immiscible blends is strongly affected by the blend morphology. Recovery after stretching of blends has been measured and the results were quantitatively related to the underlying morphological processes [36-38]. Gramespacher and Meissner reported a reversal of the recovery direction for polystyrene in poly(methyl methacrylate) blends[39]. Gronski and Lauger also observed reversal of recovery in polybutylene in polyisoprene blends; these authors

proposed that the reversal observed is related to the relaxation of the anisotropic non-equilibrium morphology[40].

Vinckier *et al.* [37] studied the effect of the underlying morphology on the recovery of an immiscible blend for slightly deformed blend morphologies as generated by steady-state shear flow and predict the scaling behavior of elastic recovery based on Palierne and Doi-Ohta theory. Vinckier *et al* [38] also systematically studied a more complex elastic recovery resulting from releasing the stress before the steady-state morphology had been reached. This was done to study the effect of the blend morphology, ranging from slightly deformed droplets to highly elongated fibrils, on the recovery behavior. A more detailed review of this research will be given in Chapter 3.

For an industrial point of view, elastic recovery is important as it affects the properties and the shape of the products. Examples of elastic phenomena during processing are extrudate swell in extrusion or distortion of injection-molded parts due to nonuniform elastic strains. Because the recoverable strains in immiscible blends can be substantial, they should be accounted for in process design.

1.3 EFFECTS OF COMPATIBILIZER

1.3.1 Compatibilizer

Surface-active species (compatibilizers) are often employed to promote intimate mixing of incompatible liquids. In the case of immiscible polymer blends, the compatibilizer may be added prior to blending or be generated by an interfacial chemical reaction during blending. Various aspects of the compatibilization of polymers have been discussed in recent reviews [41, 42].

The simplest compatibilizer is a diblock copolymer of the two components of the immiscible blend. For an immiscible blend of polymer A and polymer B, a diblock copolymer of A and B is a polymer with one long segment of polymer A joined to another long segment of polymer B. The copolymer molecule locates itself preferentially at the phase boundary between the polymer A and the polymer B phases. The block copolymers tie the two phases together, and allow energy to be transferred from one phase to the other. This helps that the minor component to improve the mechanical properties of the major component.

1.3.2 Compatibilizer Effects On Dynamics Of Drops

Compatibilizers are added to the blends to reduce the interfacial tension, and hence the work required to create new interface. This reduces the average drop size by facilitating breakup of droplets. Reduction of interfacial tension is however not the only effect of added compatibilizer [43]. Compatibilizer can also suppress coalescence of droplets[44-47], induce interfacial viscoelasticity [48, 49], and cause effects related to gradients in interfacial concentration of the compatibilizer [50, 51].

Under flow conditions, surfactants alter the interfacial stresses in a complex manner that depends on the surfactant mass transfer dynamics and amount of surfactant adsorbed. Bulk flow can also induce local gradients in compatibilizer concentration and hence in interfacial tension. This induces Marangoni stresses and differences in capillary pressure. The situation for a single drop is shown in Fig.1.6. The compatibilizer reduces the interfacial tension at the tip of the drops. The result is a complicated interplay between compatibilizer redistribution, drop deformation and bulk flows. As a result, surfactants can either reduce or enhance drop deformation under flow.

Moreover, the compatibilizer concentration gradients give rise to gradients in the interfacial tension along the surface (Marangoni stresses) that oppose deformation. Generally, Marangoni stresses reduce the interfacial velocity and cause the drops to behave as if they have higher viscosity. However, the lower interfacial tension at the tips tends to increase the overall deformation. Indeed, highly localized tip deformation can produce a shape with nearly pointed ends. Several experiments [4, 9] show that a low viscosity ratio drop, typically $p < O(0.1)$, may establish a steady deformation with a shape that has nearly pointed ends, yet very small drops are ejected from the ends. This behavior is called “tip streaming”.

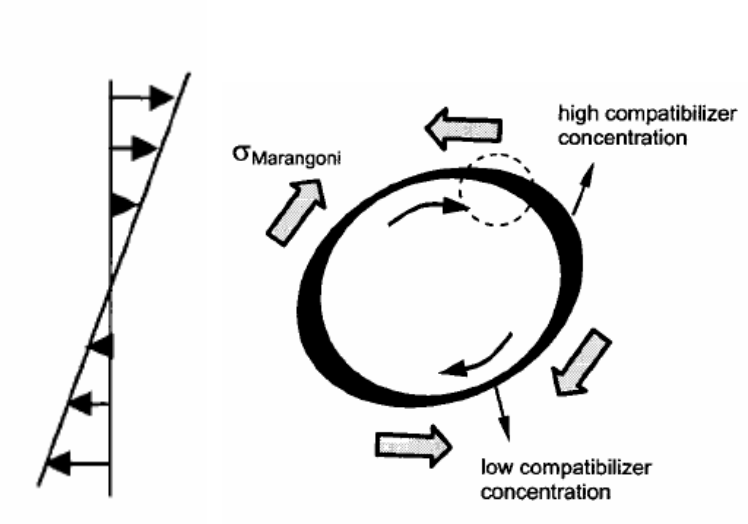

Fig.1.6 Schematic of droplets in shear flow; compatibilized droplets for finite *Ca*: interfacial contribution to stress due to both deformation and compatibilizer redistribution. Marangoni stress reduces droplet deformation. Reprinted with permission from Velankar, S. et al. [52];

An experimental study by de Bruijn [53] documents the importance of surfactants for explaining the phenomenon of tip streaming. A model study by Eggleton and Stebe [54] simulates drop breakup with compatibilizer in a linear extensional flow. The modeling results show that surface convection sweeps surfactant to the drop tips, where it accumulates and drives the surface tension to near zero; the drop assumes a transient shape with highly pointed tips; from these tips, thin liquid threads are pulled. Subsequently, small, compatibilizer-rich droplets are emitted from the termini of these threads (see Fig. 1.7).

Fig.1.7 Schematic of tip streaming: The evolution from a stable prolate spheroid to a drop undergoing tip streaming. Reprinted with permission from Stebe, K.J. et al [54].

There are some other experimental studies [51,53] that show a quantitatively and qualitatively different picture of drop deformation in presence of compatibilizer compared to the compatibilizer free case. And also numerical simulations for the dynamics of deformable compatibilizer-free drops [55-57] and compatibilizer-covered drops have been developed in attempt to elucidate the role of the compatibilizer [54, 58-61].

1.3.3 Compatibilizer Effects On Rheological Properties Of Blends

Numerical simulations suggest that with more surfactant on the drops, the viscosity of the compatibilized blend will increase, and approach that expected for rigid particles. [60, 62] in the limit of small drop deformation. It was also predicted that the contribution of the compatibilizer to steady shear properties is largest at low viscosity ratios and that the contribution to the shear stress decreases with shear rate. Thus, compatibilized blends were predicted to be shear-thinning even when their constituent drops are not significantly deformed, due to compatibilizer redistribution [60, 62].

Velankar *et al.* [51] showed that the additional contributions of the compatibilizer can be directly probed by measuring the capillary number during coalescence experiments; With the

increasing amount of compatibilizer, a systematic increase in steady shear capillary number is seen, to values well above the critical capillary number for droplet breakup of uncompatibilized systems. This indicates that a simple decrease in interfacial tension is not the only effect of adding the compatibilizer to these immiscible blends. Velankar *et al.* [52] also showed that, qualitatively, the effects of the Marangoni stress caused by flow-induced gradients in the compatibilizer are analogous to an increase in drop viscosity. At low viscosity ratios, the compatibilizer did not affect the terminal relaxation time, but increased N_1 significantly. At high viscosity ratios, the observations were exactly reversed: the terminal relaxation time increased greatly, but N_1 was not affected [52].

Interfacial viscoelasticity can be expected in compatibilizer blends. The "complete" Palierne model [27] predicts more complex behavior due to the interfacial viscoelasticity caused by the presence of compatibilizer. The main qualitative effect of interfacial viscoelasticity is an additional shoulder in the G' vs ω data. An example is shown in Fig. 4.1. This has been observed experimentally by Riemann *et al.* [48, 63] and by Van Hemelrijck et al. [64]. Starting with the complete Palierne model and making some simplifying assumptions, those authors were able to fit the model to their data and obtain the viscoelastic properties of the interface.

2.0 EXPERIMENTAL

2.1 EXPERIMENTAL MATERIALS

All experiments were performed on a blend of polyisobutylene (PIB, Mw 1300, Parapol from Exxon Chemicals) dispersed in polydimethylsiloxane (PDMS, $M_w \approx 135000$, Rhodosil V 100000 from Rhodia Chemicals). This blend system has also been used by other researchers[28-30, 32, 51, 65-67] to study the rheology and morphology of immiscible blends.

The viscosity of the pure components at different temperatures at 120 Pa shear stress is listed in Table 2.1. These components have been chosen because at room temperature they have a viscosity comparable to that of typical commercial polymers under processing conditions. However, unlike commercial polymers, both polymers show a constant shear viscosity over the range of stresses investigated.

Table2.1 Pure components shear viscosity at different temperature at 120 Pa shear stress

	Viscosity at 120 Pa shear stress Pa.s		
Pure components	17°C	23°C	32°C
PIB (drop phase)	181	101	46
PDMS (matrix phase)	106	94	159
Viscosity ratio	1.70	1.10	0.29

Dynamic oscillatory experimental tests were conducted for both components. Fig. 2.1 shows that $G'' >> G'$ for both components at low frequencies. Fig. 2.2 shows that $|\eta^*|$ is almost independent of ω below $\omega = 10$ rad/s for both PIB and PDMS. Recovery from 120 Pa stress is negligible for PIB while PDMS has very little recovery (~ 1% strain) as the raw data in Fig. 2.3 shows. Thus, we conclude that PIB is Newtonian and PDMS is nearly Newtonian under experimental conditions.

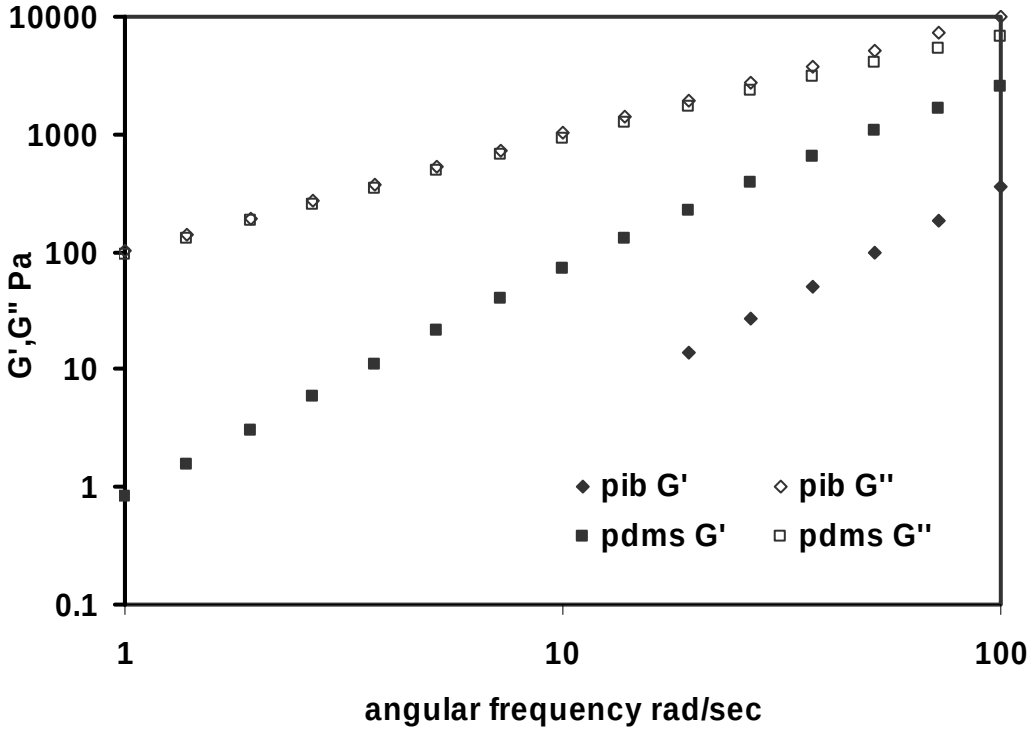

Fig. 2.1G' and G" of PIB and PDMS at 23°C.

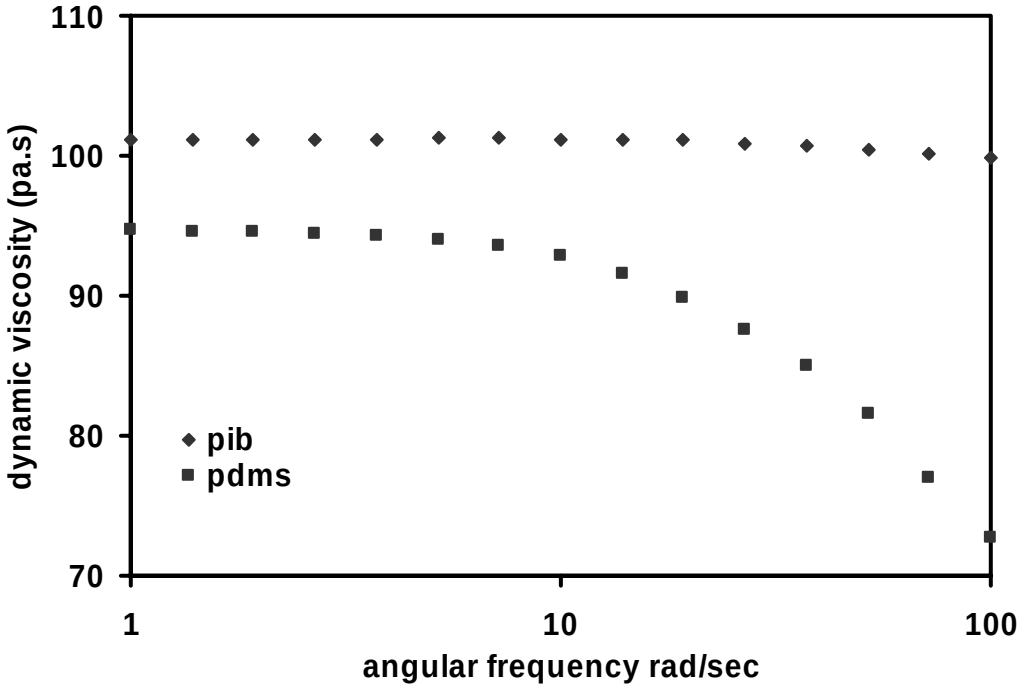

Fig.2.2 Dynamic viscosity of PIB and PDMS at 23°C

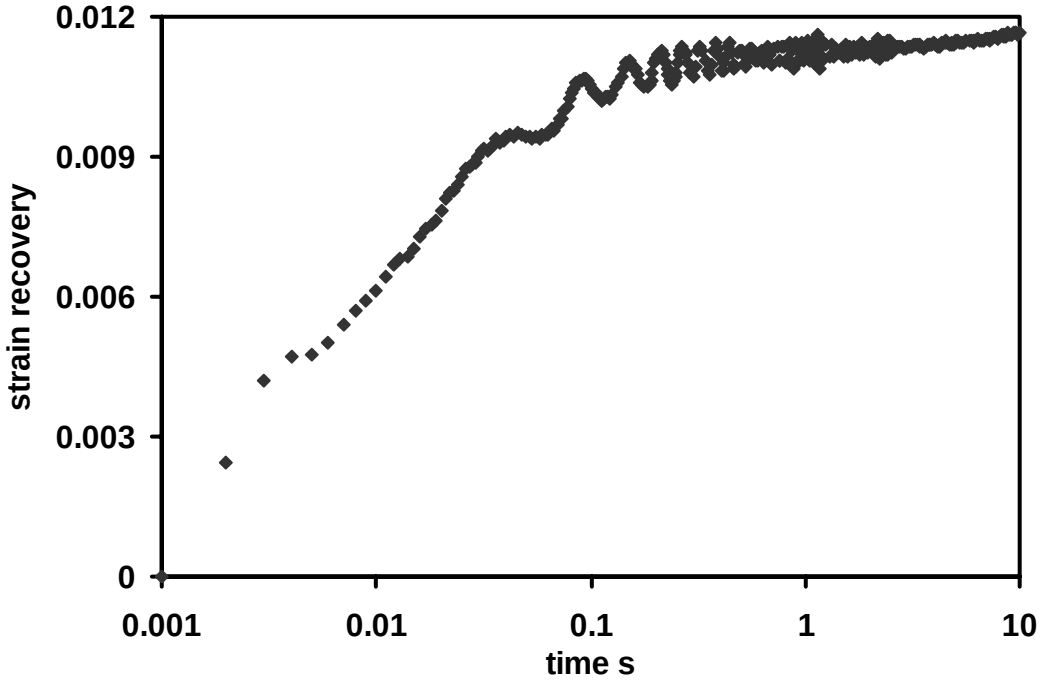

Fig.2.3 Strain (creep) recovery of PDMS after cessation of shear at 120 Pa and 23°C (The recovery of PIB is too small to be measured accurately)

As the pure components show very little viscoelasticity, the elastic recovery of the blend can be almost completely attributed the retraction of the interface. The interfacial tension between pure components has been measured by using various techniques and the results obtained at 23°C range from 2.1 to 3.4 mN/m [68].

A diblock copolymer of PIB and PDMS ($M_{w,PIB} \approx 6150$; $M_{w,PDMS} \approx 8000$; polydispersity ≈ 1.3) was synthesized by Polymer Source Inc. It was made available for this research by the Laboratory of Applied Rheology at the K.U. Leuven, Belgium. The low molecular weights of the

blocks imply that there are no entanglements between the blocks and the bulk phases. Details of this block copolymer are given by Velankar *et al*. [69].

2.2 BLENDS PREPARATION

Blends were prepared by mixing the diblock copolymer into PIB to obtain the dispersed phase, and then blending this mixture into the PDMS matrix. All mixing was performed by hand with a spatula. The entrapped air bubbles were removed by keeping the sample overnight in a vacuum oven. The volume percentage of the component in the blend is expected to be quite close to the weight percentage due to the small density difference between components (ρ_{PIB} 895.3 kg/m^{3}and ρ_{PDMS} 975.0 kg/m^3 at 23°C [70]). The amount of diblock is quoted as a weight percentage of the total.

2.3 EXPERIMENTAL PROCEDURE

The flow protocol for tests of recovery of blends with and without compatibilizer with the steady flow histories is depicted in Fig. 2.4. It involves preshearing at high shear stress (480 Pa) for 3000 strain units, followed by shearing at 120 Pa till steady state is reached. Flow is intermittently arrested, typically for 5-10 minutes, to measure strain recovery. For blends with low drop weight fraction (10%), the dynamic moduli are also measured immediately after the recovery by a oscillatory frequency sweep. For large weight fractions, dynamic oscillatory experiments were not performed due to changes in morphology during oscillatory tests.

The flow protocol for the test of recovery of blends with the transient flow histories is depicted in Fig. 2.5. A steady shear stress (30 Pa) is applied followed by a higher shear stress (120 Pa) for a short period to develop different morphologies. Recovery of strain is then measured.

2.4 RHEOLOGY MEASUREMENT

Rheological measurements were performed on a TA instrument AR2000 stress rheometer using 40 mm diameter, 1° cone and plate geometry. The temperature is controlled by a Peltier plate with an accuracy of +/- 1ºC. Only the temperatures in Table 2.1 were used.

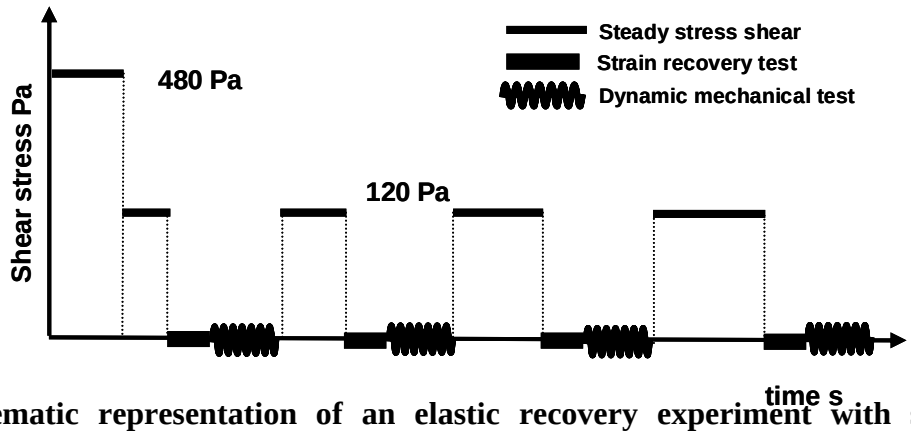

Fig.2.4 Schematic representation of an elastic recovery experiment with steady flow histories. (For weight fraction of drops exceeding 10%, the dynamic tests were not conducted).

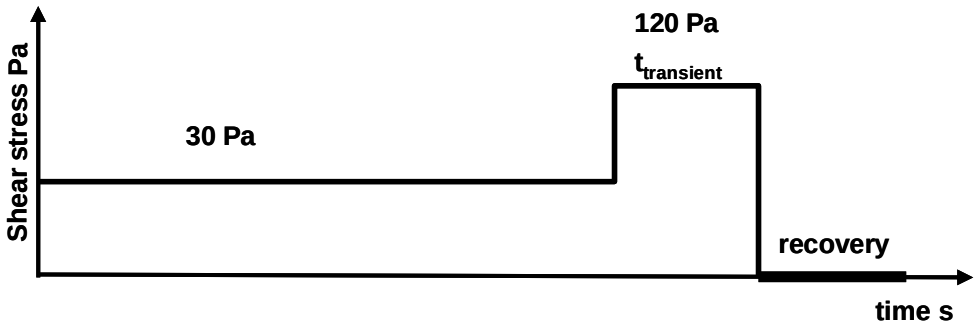

Fig.2.5 Schematic representation of an elastic recovery experiment with transient flow histories.

3.0 EXPERIMENTAL RESULTS AND DISCUSSION FOR UNCOMPATIBILIZED BLENDS

3.1 INTRODUCTION

While the motivation for this thesis was the effect of added compatibilizer on the strain recovery of immiscible blends, several "baseline" measurements on strain recovery of blends without compatibilizer were conducted. Here we summarize the observations of the creep recovery after cessation of steady shear of uncompatibilized blends with droplet-matrix morphologies. Our results add significantly to the data on recovery of immiscible blends, in particular, we are unaware of any previous publications that detail the effects of volume fraction and viscosity ratio of the drops on the creep recovery.

3.2 THEORY

An excellent summary of the theory of creep recovery of droplet-matrix blends has been given previously. Briefly, when under shear, droplets are deformed and partially oriented along the flow direction. Upon cessation of shear the droplets retract back to their spherical shape. This retraction drives strain recovery of the blend; clearly if the drops are highly deformed and oriented prior to cessation of shear, a larger recovery is expected. As has been emphasized in

previous work on immiscible blends of model Newtonian components, this recovery is driven by the interface and not by the bulk fluids.

A simple model of recovery of droplet-matrix blends in the linear viscoelastic regime was proposed recently based on older results of Graebling [22, 37]. Treating the blend with a Jefferys model, it was concluded that the recovery follows simple exponential kinetics:

$$\gamma = \gamma_\infty[1-\exp(-t/\tau_2)] \tag{3-1}$$

where

$$\gamma_\infty = \frac{stress}{\eta}[\tau_1 - \tau_2] \tag{3-2}$$

τ_1 and τ_2 are the relaxation time and the retardation time respectively, and γ_∞ is the ultimate recovery. Both τ_1 and τ_2 have a similar form:

$$\tau_1 = \frac{R\eta_m}{\sigma} g(p,\phi) \quad \text{, and} \quad \tau_2 = \frac{R\eta_m}{\sigma} h(p,\phi) \tag{3-3}$$

where g and h are functions given below. These times can be made dimensionless by multiplying by the shear rate prior to cessation of shear:

$$\tau^*_1 = \tau_1 \dot{\gamma} = \frac{\dot{\gamma} R\eta_m}{\sigma} g(p,\phi) = Cag(p,\phi) \tag{3-4}$$

Similarly

$$\tau^*_2 = \tau_2 \dot{\gamma} = Ca\ h(p,\phi) \tag{3-5}$$

Where the capillary number, Ca, of the drops is gven by eq.1-1

$$Ca = \frac{\dot{\gamma} R \eta_m}{\sigma} \tag{3-6}$$

Similarly, Eq. 3-2 can be rearranged in a dimensionless form:

$$\gamma_\infty = \frac{\dot{\gamma} \eta_b}{\eta_b} \frac{R \eta_m}{\sigma} [g(p,\phi) - h(p,\phi)] = Ca[g(p,\phi) - h(p,\phi)] \tag{3-7}$$

Thus, as per the Vinckier model [37], the ultimate recovery and the dimensionless retardation time are both proportional to the Ca prior to cessation of shear, with additional dependences on viscosity ratio and volume fraction. The functions g and h have been given by Graebling [20]

$$g(p,\phi) = \frac{19p+16}{4}\left[\frac{2p+3-2\phi(p-1)}{10(p+1)-2\phi(5p+2)}\right] \tag{3-8}$$

$$h(p,\phi) = \frac{19p+16}{4}\left[\frac{2p+3+3\phi(p-1)}{10(p+1)+3\phi(5p+2)}\right] \tag{3-9}$$

It is convenient to expand these expressions in powers of ϕ

$$g(p,\phi) = \frac{19p+16}{40(p+1)}\left[2p+3+\frac{19p+16}{5(p+1)}\phi + \frac{(19p+16)(5p+2)}{25(p+1)^2}\phi^2\right] \tag{3-10}$$

$$h(p,\phi) = \frac{19p+16}{40(p+1)}\left[2p+3-\frac{3(19p+16)}{10(p+1)}\phi + \frac{9(19p+16)(5p+2)}{100(p+1)^2}\phi^2\right] \tag{3-11}$$

Where terms of ϕ^3 and higher order have been neglected. Retaining only the terms up to the first order in ϕ gives the same expressions as Oldroyd [26]. Substituting the expanded Eqs. 3-10 and 3-11 into Eq.3-7 we obtain

$$\gamma_\infty = Ca\frac{1}{80}\left(\frac{19p+16}{p+1}\right)^2\left[\phi - \frac{1}{10}\frac{5p+2}{p+1}\phi^2\right] \tag{3-12}$$

A major goal of this chapter is to test Eq. 3-11 and 3-12.

Finally, Taylor's [4] theory predicts that at small Ca, the deformation of the drops is given by

$$D = Ca\frac{19p+16}{16(p+1)} \tag{3-13}$$

Thus,

$$\gamma_\infty = D\frac{1}{5}\left(\frac{19p+16}{p+1}\right)\left[\phi - \frac{1}{10}\frac{5p+2}{p+1}\phi^2\right] \tag{3-14}$$

The ultimate recovery is thus proportional to the deformation. Some noteworthy features of the above equations are:

- The absolute value of drop size does not appear in any of the above equations: all properties can be expressed in dimensionless form.
- The ultimate recovery in Eq. 3-12 is weakly dependent on p. This is directly attributable to the weak dependence of D on p of Eq. 3-13 [4]
- The coefficient of ϕ^2 in Eq. 3-12 is negative; the recovered strain is predicted to increase slower than the volume fraction due to pairwise drop interactions.
- The coefficient of ϕ in Eq. 3-11 is also negative; the dimensionless retardation time reduces as the volume fraction of the drops increases.

It must be emphasized that Eq. 3-11 and 3-12 have a strong dependence on Ca and therefore testing the dependence of the ultimate recovery and the retardation time on ϕ requires Ca to be kept constant, which is difficult do experimentally unless coalescence is very slow.

3.3 RESULTS

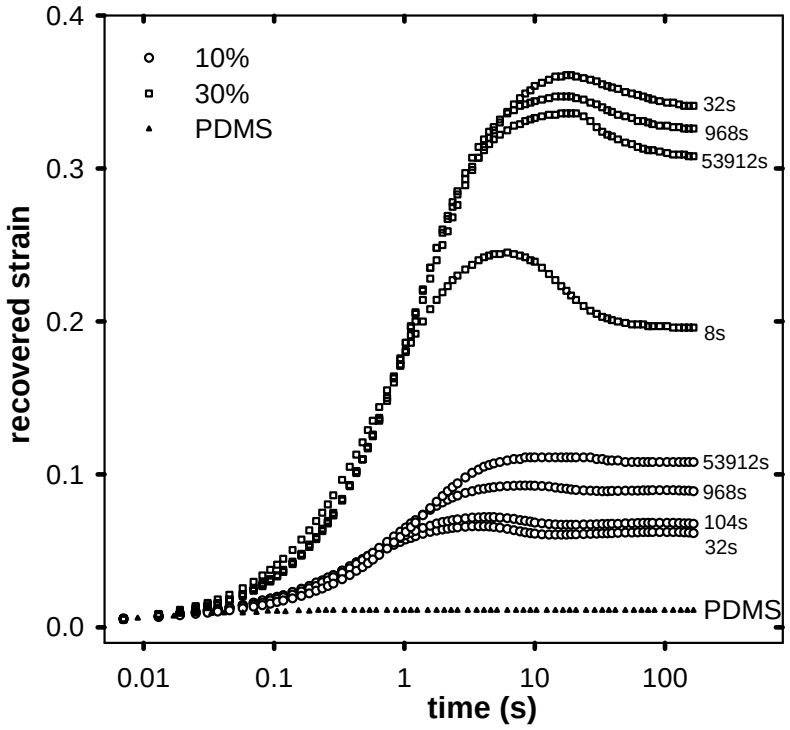

Fig.3.1 Recovery of blends with viscosity ratio 1.1 and 10 wt % or 30 wt % drops at various times after stepping down the shear stress to 120 Pa.

Fig. 3.1 shows the creep recovery of blends with 10% and 30% drops after shearing at 120 Pa for the various times specified in the figure. The recovery of matrix phase PDMS is also plotted for comparison (the recovery of the PIB was too small to be measured). The blends show

significantly more recovery than the components. While the ultimate recovery and the time required for recovery vary with the volume fraction and viscosity ratio of the drops, the shape of the curves are quite similar for all uncompatibilized blends. They are also similar to the recovery results for similar blends published previously [26]. For the blends with 10% dispersed phase, the recovered strain and the time for recovery increase with increasing shearing time. This can be understood easily: upon reducing the stress to 120 Pa, drops grow by coalescence and are more deformed, and hence the blends show more recovery. A remarkable feature of Fig. 3.1 is that for blends with 30% drops, the ultimate recovery at very short shearing times is maximum, and then reduces to its steady value. Such a phenomenon cannot be explained by a monotonic increase in drop size and we have no explanation of this result.

A slight reversal of recovery is evident for these blends, especially at short shearing times. Vinckier *et al*. [37] claimed that they did not observe reversal of recovery in similar blends, yet, weak reversal is evident in their own data (see Fig. 3 in Vinckier *et al.* [37]). Far stronger reversal of recovery in two-phase blends was first documented by Gramespacher and Meissner [39], with up to a third of the maximum recovery being reversed. Vinckier *et al.* [37] have discussed previously why similarly strong reversal of recovery is not seen in the model blends studied here. Reversal of recovery is not discussed further in this chapter.

Fig. 3.2 replots the data of Fig.3.1 for both volume fractions after shearing for very long times (i.e. to steady state; see below) on a log-log scale. The recovery of matrix phase PDMS is also plotted for comparison. It is evident that much of the recovery occurring prior to 0.1 s is attributable to recovery of the matrix phase PDMS. Since we are interested primarily in the

recovery that is attributable to interface, this "component contribution" must be subtracted from the blend recovery. Following Vinckier et al [37] we do this in a simple-minded fashion. The quantity of interest, viz. the interfacial contribution to the recovery, $\gamma(t)$ is obtained by simply subtracting the volume average contribution of the components:

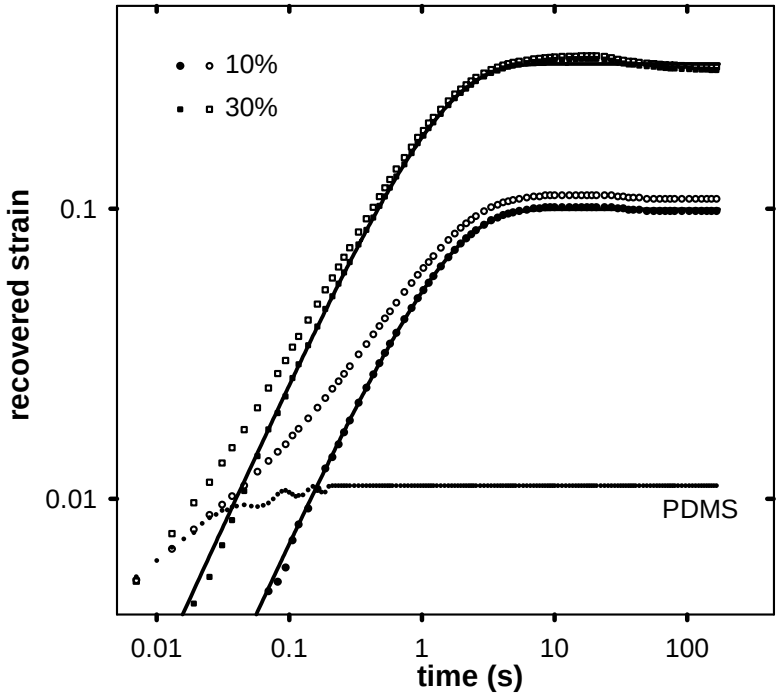

Fig.3.2 Data analysis of recovery curves: Open symbols: "raw" recovery data; these are the same data labeled "53912" in Fig. 3.1. Filled symbols: recovery after subtraction of component contribution as per Eq. 3.12. Solid lines: fits to single exponential kinetics Eq. 3.1.

$$\gamma(t) = \gamma_{total}(t) - \sum \phi_i \gamma_i(t) \approx \gamma_{total}(t) - \phi_{PDMS}\gamma_{PDMS}(t) \qquad (3\text{-}14)$$

where the second part of this expression is justified by the fact that the PIB phase shows negligible recovery. While this equation is not rigorous, the errors involved are expected to be small due to the nearly-Newtonian nature of the pure components. After subtraction of the component contribution, the remaining recovery, which is attributable to interfacial tension, appears to be of a very simple nature. Indeed, a simple exponential (Eq.3-1) appears to fit the recovery reasonably well (except the slight reversal of recovery, which obviously cannot be captured by any exponential decay). Henceforth in this chapter, we will only discuss the subtracted curves, i.e. the interfacial contribution to the recovery as defined by Eq.3-12. The subtracted curves allow us to obtain two quantities: the interfacial contribution to the recovered strain, and the timescale of the interface-driven recovery process, i.e. the retardation time. The latter is obtained by fitting single exponential curves as shown in Fig.3.2. It is then made made dimensionless by multiplying by shear rate. The ultimate recovery and the dimensionless retardation time are plotted in Fig. 3.3a for the blends with 10 wt % drops and Fig. 3.3b for blends with 30 wt % drops.

For the blends with 10% of the dispersed phase, we were also able to conduct dynamic oscillatory measurements immediately following the recovery; at the higher volume fractions, rapid quiescent coalescence did not permit obtaining the dynamic mechanical properties. The characteristic relaxation time was calculated from storage modulus G' of the blends (see Appendix A). This time is related to the capillary number by Eq. 3-6. Thus, the Ca of the blends immediately prior to recovery can be obtained from the dynamic oscillatory measurements. We estimate systematic errors up to 10% i.e. all the Ca values for a given blend can be varied by up to 10% with no visible degradation in quality of fits.

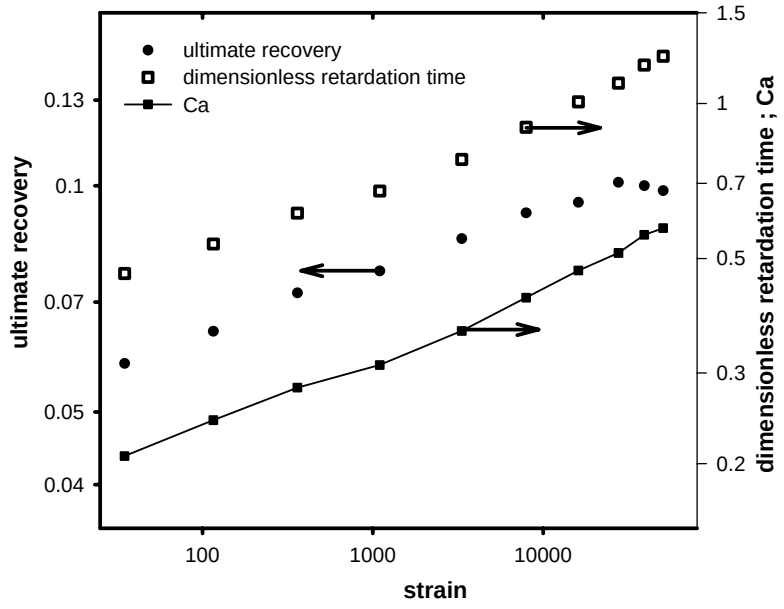

(a)

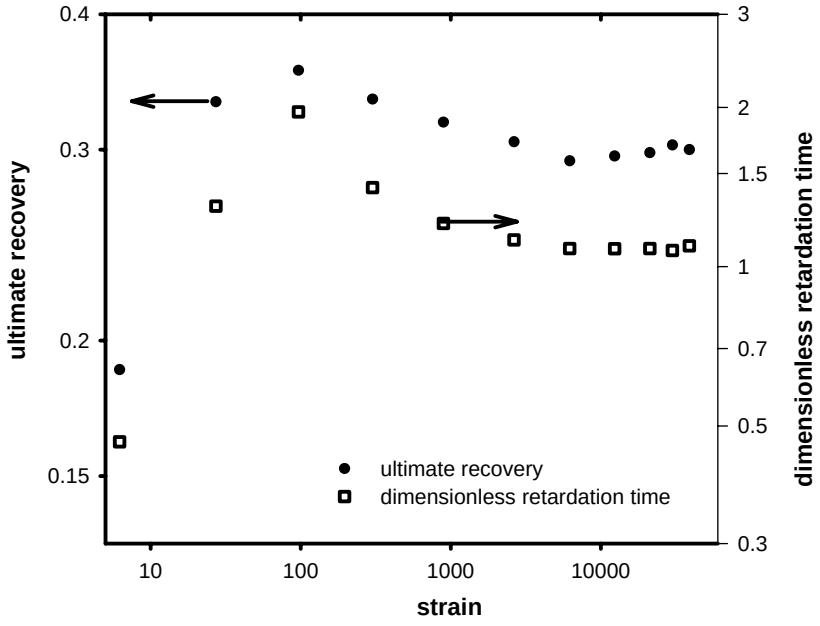

(b)

Fig.3.3 Ultimate recovery and dimensionless retardation time for blends with viscosity ratio 1.1 and (a) 10% drops, and (b) 30% drops at various times after stepping down shear stress to 120 Pa.

These Ca values are also plotted in Fig 3.3. It is evident that the values of Ca, the ultimate recovery and dimensionless retardation time show the same trend. Past authors have used the leveling off of the Ca vs strain to determine that the blends have reached steady shear conditions[51, 52, 64]. Fig. 3.3 shows that leveling off of the retardation time or ultimate recovery is an equally valid criterion. The creep recovery is however more convenient to use since it can be measured much more quickly, and even for blends with high drop volume fraction.

The data of Fig. 3.3a are replotted in Fig. 3.4 and compared with the prediction of Eqs. 3-11 and 3-12. Only terms up to first order in ϕ have been retained. Above it was mentioned that there is up to 10% systematic error in the Ca values; thus, all the points at a particular viscosity ratio could be moved to the right or left by up to 10%. Nevertheless it is clear that the Eq.3-11 is able to predict the retardation time reasonably well, whereas Eq. 3-11 significantly overpredicts the ultimate recovery. Including terms with higher order in ϕ do not change these conclusions significantly. In contrast Vinkier *et al* [37] concluded that Eq. 3-12 worked well for one specific blend at a viscosity ratio of 1. It must be emphasized however that Vinckier *et al* obtained the Ca by a completely different method: microscopic measurements of drop size and independent measurements of interfacial tension were used in Eq. 3.5 to calculate Ca.

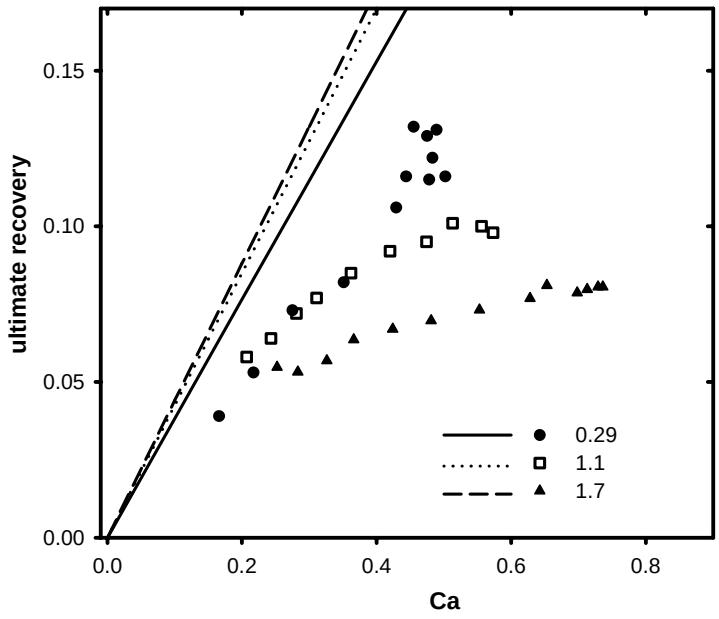

(a)

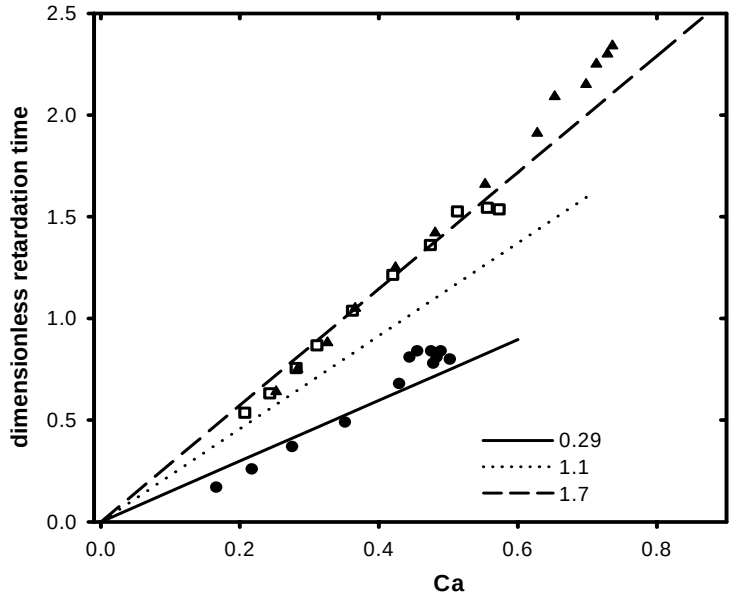

(b)

Fig.3.4 (a) Ultimate recovery, and (b) dimensionless retardation time of blends at various viscosity ratios and with 10% drops. Lines represent Eqs. 3-4 and 3-11 in (a), and Eq. 3-10 in (b), both with only terms up to first order in ϕ.

Secondly, while the theory predicts a weak increase in the ultimate recovery with viscosity ratio, the data show that ultimate recovery decreases strongly with increasing viscosity ratio. This is probably due to fact that the theory assumes slightly deformed drops and hence is valid at only small Ca. In contrast, at large Ca, drops with low viscosity are known to deform significantly more [71].

Finally, even with the 10% systematic error in Ca, it is clear that the ultimate recovery vs. Ca curves have qualitatively different shapes at different viscosity ratios: for $p > 1$, the curves are convex-up and γ_∞ appears to level off at high Ca, whereas for $p < 1$, the curve is convex-down and γ_∞ appears to increase sharply above Ca=0.4. We propose that this is due to the increasing deformation of low viscosity ratio drops as Ca increases. Indeed Maffetone and Minale proposed a model of drop deformation recently to capture exactly this phenomenon [71]. If the deformation predicted by the Maffetone-Minale model is used in Eq. 3-13, the convex-up vs convex-down trends of the ultimate recovery vs. Ca curves at various viscosity ratios can be captured, however, the ultimate recovery is still overpredicted.

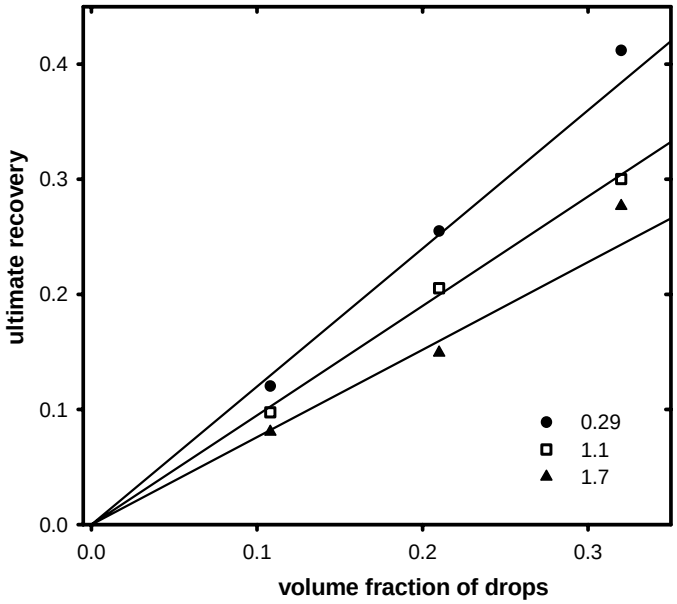

(a)

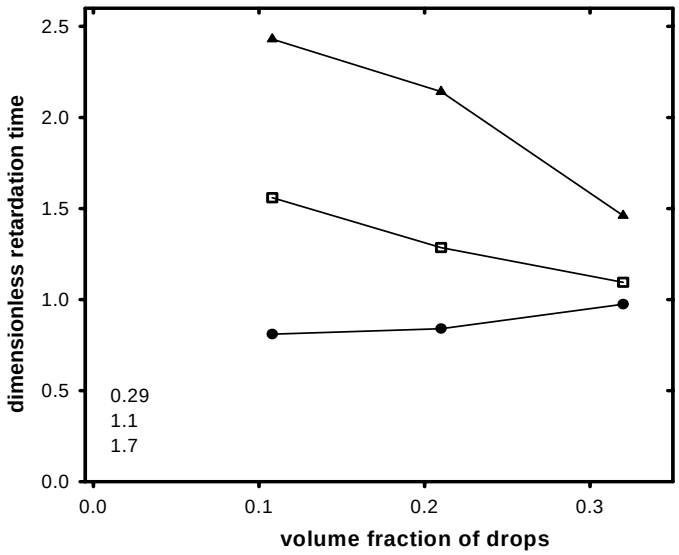

(b)

Fig.3.5 Dependence of (a) ultimate recovery, and (b) dimensionless retardation time, on volume fraction of the dispersed phase at various viscosity ratios. In (a), straight lines are only guides to the eye.

Finally, the ultimate recovery and the dimensionless retardation time are plotted as a function of volume fraction in Fig 3.5. For the p=1 blend, recovery is nearly proportional to volume fraction. For p=0.29 and 1.7, recovery is seen to grow faster than ϕ. At first glance this seems to contradict Eq. 3-12 in which the coefficient of ϕ^2 is negative. However, since we are considering steady shear recovery, the steady shear Ca itself changes with ϕ, therefore a straightforward comparison with Eq. 3-12 is not possible. The retardation time for the p=1.7and p=1.1 blends decreases with droplets fraction seemingly in agreement with Eq. 3-11, but that of the p=0.29 blends increases. Once again, since the steady shear Ca itself changes with droplets fraction, a direct comparison with Eq. 3-11 is not possible.

4.0 EXPERIMENTAL RESULTS AND DISCUSSION FOR COMPATIBILIZED BLENDS

4.1 INTRODUCTION

Immiscible homopolymers are often blended mechanically to obtain blends with properties significantly superior to those of the component polymers. The creep recovery of such blends was studied in the last chapter. Surface-active compatibilizers are commonly used to improve blending of immiscible homopolymers. The creep recovery of blends with compatibilizer are considered here.

Velankar *et al.* [52] studied the steady shear rheological properties of the same system previously. It was observed, qualitatively, at low viscosity ratios, the compatibilizer did not affect the terminal relaxation time, but increased N_1 significantly. At high viscosity ratios, the observations were exactly reversed: the terminal relaxation time increased greatly, but N_1 was not affected [52].

The goal of this research is to address the following questions: How does a small amount of surfactant affect the creep recovery of droplet-matrix blends? How does the effect of the surfactant vary with viscosity ratio? Considering that samples with very small amounts of

compatibilizer can show two relaxation processes, is their creep recovery still a single retardation process?

4.2 EXPERIMENTAL OBSERVATIONS

4.2.1 Recovery After Cessation Of Steady Shear

The rheological properties of uncompatibilized blends were discussed in last chapter. Compatibilized blends show many of the same features, at least qualitatively. These are discussed first:

- The recovery curves of compatibilized blends are qualitatively similar to those of uncompatibilized ones (see Fig. 3.2). In particular, most of the recovery prior to 0.1 s is attributable to the recovery of the matrix phase PDMS. We can therefore extract the interfacial contribution to the recovery by simply subtracting the volume average of the recovery of the components from that of the blends (Eq. 3-14).

- Most compatibilized blends show a slight reversal of recovery similar to that seen for uncompatibilized blends (see Fig. 3.1). The amount of strain recovery reversed is comparable to that for blends without compatibilizer (~0.02) but the reversal takes a much longer time when compatibilizer is added.

- Upon stepping down the shear stress from 480 Pa to 120 Pa, the ultimate recovery of the blends with 10% drop phase increases significantly. A plot of the

ultimate recovery vs the total strain applied at 120 Pa looks very similar to Fig. 3.3.

- Moreover, for compatibilized blends with 10% drops, the terminal relaxation time obtained from dynamic oscillatory experiments shows the same trend as the ultimate recovery. Thus, whether steady shear conditions have been reached or not can be judged equally well by either the ultimate recovery or the terminal relaxation time. For uncompatibilized blends however, we were able to convert this terminal relaxation time into a capillary number, and thus plot Fig. 3.4. For compatibilized blends, the terminal relaxation time cannot simply be converted into a Ca because Eq. 3-6 is not valid for compatibilized blends.

- For blends with 20% or 30% drops, a plot similar to Fig. 3.3b is obtained i.e. at very short shearing times, the ultimate recovery and retardation time are maximum and they reduce to their steady state values. Once again, we propose no mechanism to explain this observation.

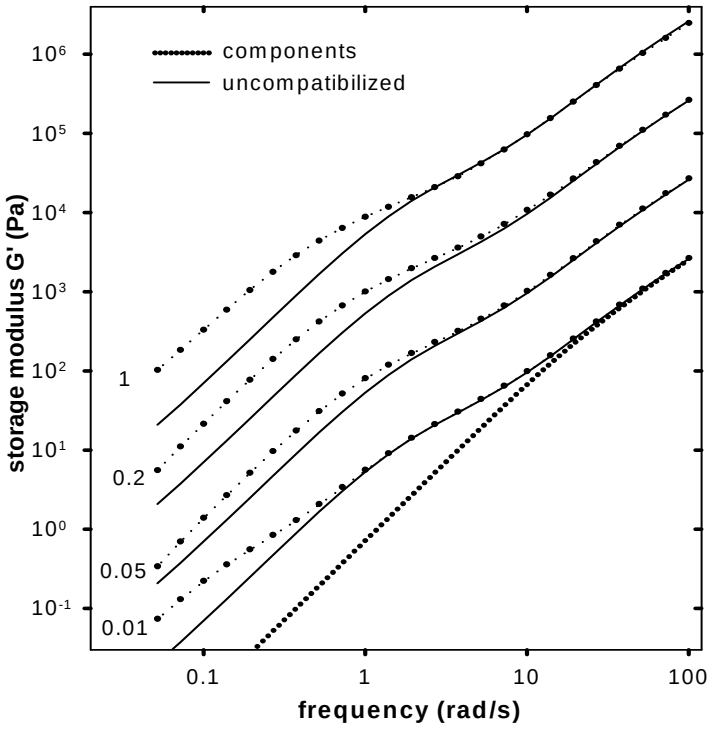

Fig.4.1 Dynamic oscillatory moduli of blends with compatibilizer (wt%): at the end of preshearing; right after shearing to steady state at 120 Pa.

The differences between blends with and without compatibilizer are now considered. Fig. 4.1 plots the frequency sweep results of the p=1.1 series of blends with 10% drops. We can find a weak second shoulder developing at very low frequencies for blends with 0.01% compatibilizer. As the sample was sheared at 120 Pa, the shoulder at higher frequency moved to lower frequency, but the low frequency shoulder was not significantly affected. As a result, it becomes difficult to identify the two shoulders separately as was also observed elsewhere [64]. The principal conclusion is that compatibilized blends can show two distinct relaxation processes.

In what follows, only the recovery after reaching steady shearing conditions will be discussed. Figure 4.2 plots the recovery of the blends with a viscosity ratio of 1.1, 10% or 30% drops, and various amounts of compatibilizer. Two features are noteworthy. Firstly, the addition of compatibilizer increases the recovered strain significantly (this is clearer in Fig. 4.3a). Secondly, single-exponential kinetics can no longer capture accurately the recovery of blends with large amount of compatibilizer. Interestingly enough, while the two relaxation processes are most clearly visible at the lowest compatibilizer level, the worst fits to the single-retardation time model occur at the highest compatibilizer levels.

Unfortunately, we are unable to obtain the two retardation times quantitatively. The chief problem is that except at 1% compatibilizer, the two retardation times are not well-separated and simple fitting methods are inadequate to obtain the two times reliably. Non-linear regularization procedures may be able to obtain two retardation times reliably, but these were not attempted. In the remainder of this paper, we will therefore persist with single-exponential fits to obtain a single retardation time for each curve. While the fits are sometimes poor, these times are useful practically, since they capture the main features of the recovery kinetics (e.g. they track the time for completing half of the recovery very well) and hence allow us to comment on the effect of compatibilizer. As in Chapter 3, these times are multiplied by the shear rate prior to recovery to render them dimensionless. A clearer separation of the retardation times may be achievable on the system used by Van Hemelrijck *et al.*[64] in which the two shoulders in G′ are considerably more distinct.

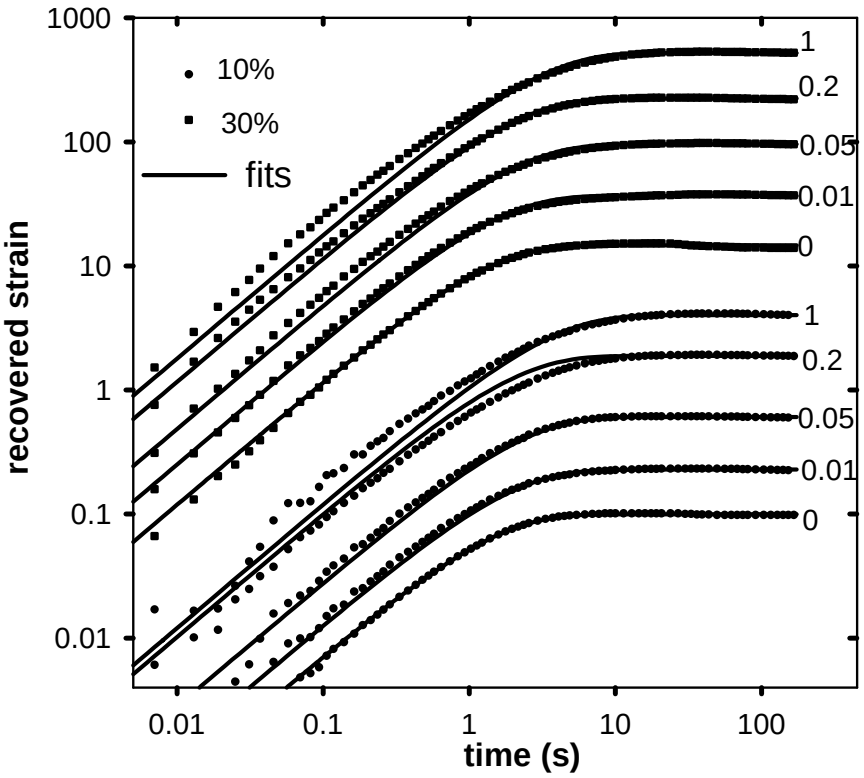

Fig.4.2 Recovery of blends with viscosity ratio 1.1, 10% or 30% drops, and various levels of compatibilizer given as weight% of the blend. Each curve is shifted upwards by one-third log unit for clarity. Solid lines are best fits of single exponential recovery kinetics to the data for time > 0.02 s.

In the remainder of this section, the two important quantities upon cessation of steady shear are considered: ultimate recovery and dimensionless retardation time. These are plotted in Fig. 4.3 for the blends with viscosity ratio 1.1. The compatibilizer is seen to increase the ultimate recovery of the blends as well as increase the dimensionless retardation time. The effect of compatibilizer is not subtle; even the addition of as little as 0.2% compatibilizer increases the ultimate recovery and the dimensionless retardation time by more than 50%.

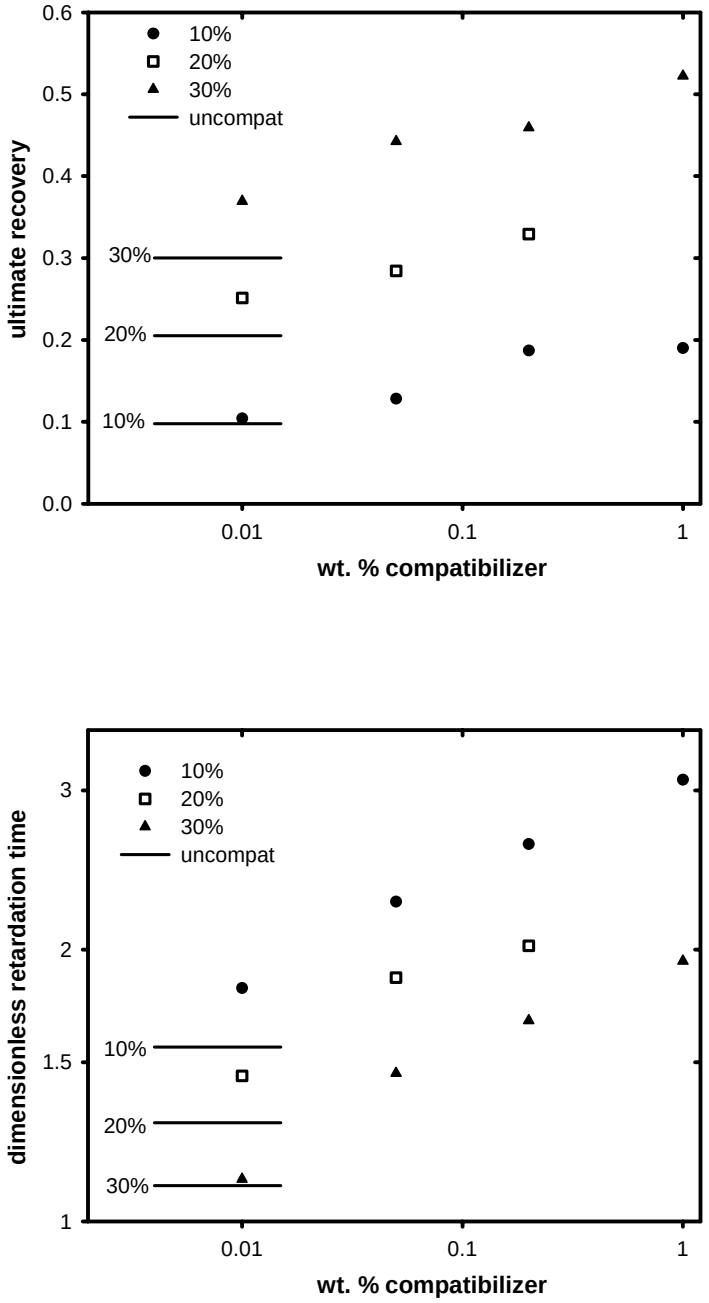

Fig.4.3 Dependence on the concentration of compatibilizer of (a) ultimate recovery, and (b) dimensionless retardation time, of blends with viscosity ratio 1.1, and 10, 20 or 30 wt % drops after reaching steady shear at 120 Pa. The retardation times at high compatibilizer content are approximate due to poor fits to the recovery curves.

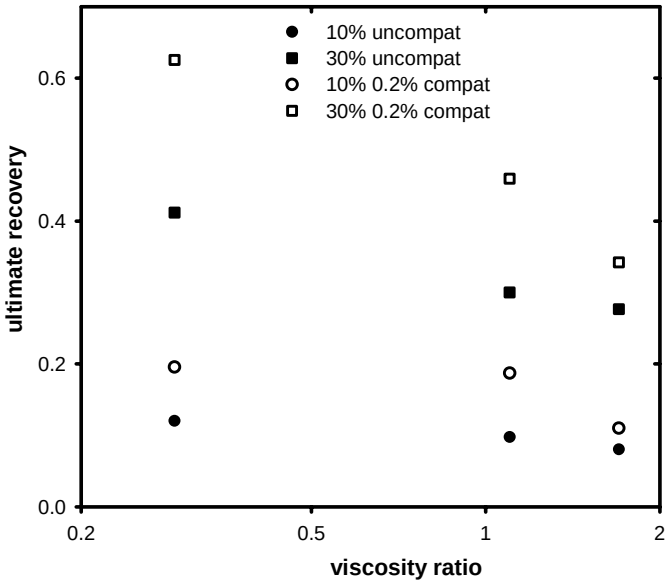

(a)

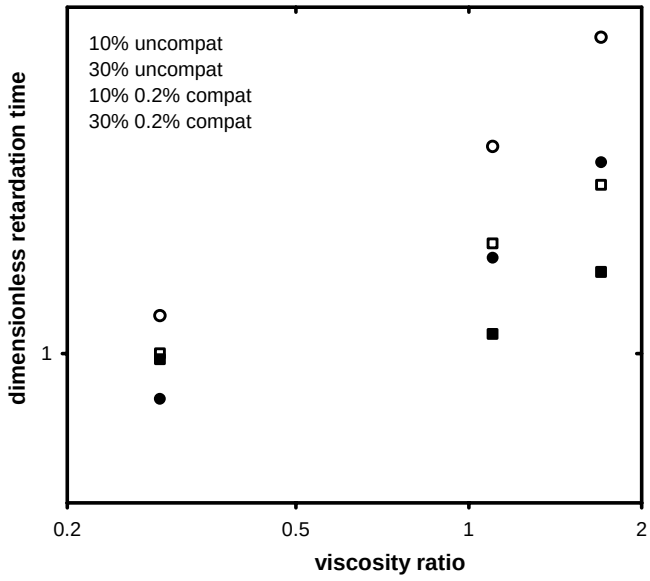

(b) (the symbols represent same volume fractions as a)

Fig.4.4 Dependence on viscosity ratio of (a) ultimate recovery, and (b) dimensionless retardation time, of blends with 10or 30 wt % drops with and without compatibilizer after reaching steady shear at 120 Pa.

Finally, the effects of volume fraction at fixed viscosity ratio (not plotted) are similar to those of uncompatibilized blends:

- the ultimate recovery under steady shear conditions increases with volume fraction of the drops at all compatibilizer levels. As in uncompatibilized samples, the increase is nearly proportional to ϕ, or slightly faster.
- the retardation time reduces with increasing volume fraction of drops at all compatibilizer levels (except for the uncompatibilized sample p=0.29 as shown in Fig.3.5b).

4.2.2 Recovery After Cessation Of Brief Shearing

As discussed in last chapter, in blends without compatibilizer, recovery is driven by the relaxation of deformed drops. Steady state deformation of drops increases with capillary number, hence the strain recovered and the retardation time increases with capillary number. However, only modest deformations can be realized under steady shear conditions because the steady-state Ca that can be applied is limited to values below the critical Ca for breakup. Under transient flow conditions however, very large drop deformations can be realized. Vinckier *et al.*[38] considered recovery of morphologies with such highly deformed drops. Blends were presheared at low stresses to allow large drops to be formed by flow-induced coalescence. They were then sheared briefly at high Ca to deform the drops, and recovery was measured. Recovery was found to be very large under short shearing times. Here we examine effects of compatibilizer under such conditions.

Fig. 4.5 shows some of the recovery curves after transient shear. Blends with 30 wt % drops were sheared at 30 Pa for 2000 strain units, which is sufficient for them to be close to their steady state morphology. They were then sheared at 120 Pa for brief periods denoted by t_s to achieve a strain of γ_s, and then allowed to recover. Comparing the recovery curves for the uncompatibilized blend at various values of t_s, it is immediately evident that the ultimate recovery and the time required to complete the recovery first increases and then decreases with increasing t_s. A single retardation time can still approximate the recovery process although the fits are not very good especially at $t_s \sim 40$. At the longest value of t_s studied (3600 s, not shown), the recovery curve is nearly identical to the steady shear recovery curve (Fig.4.2).

For samples with compatibilizer, the same observations hold, however the single exponential fits are generally poorer at all times. Indeed it was noted in the last chapter that even under steady shear conditions, a single retardation time was insufficient to capture the recovery process. The addition of compatibilizer increases the ultimate recovery at all values of t_s. Moreover, a qualitatively new phenomenon is evident in the data: at very long times, a slow retardation process is evident at small value of t_s. This is most clearly visible at $t_s = 2$ s and 4 s for the 0.2% compatibilized sample (Fig.4.5b) but similar slow retardations are evident at other values of t_s and at other compatibilizer levels. This slow process is quite weak: the ultimate recovery during this process is less than 0.02. The slow retardation is no longer obvious at larger t_s, however, the reversal of recovery comes into play so it is entirely possible that such a weak but slow recovery occurs in all compatibilized samples but is simply overwhelmed by the reversal of recovery under most circumstances.

(a)

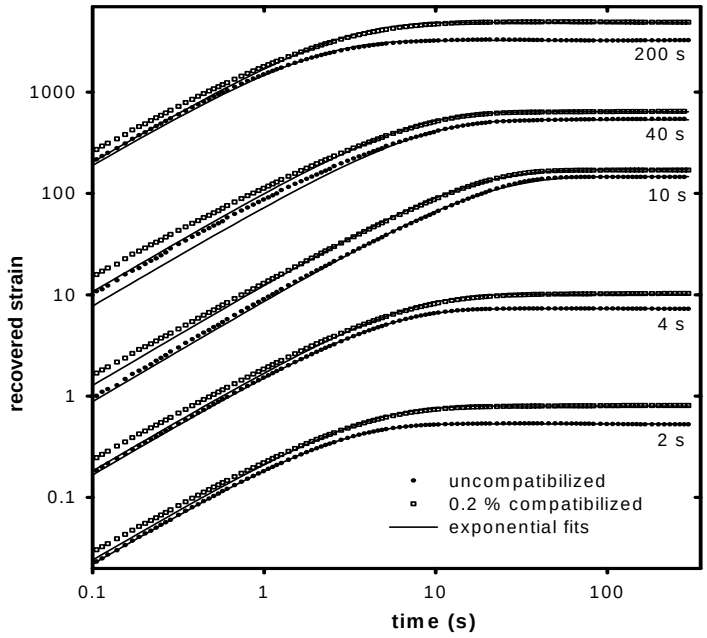

(b)

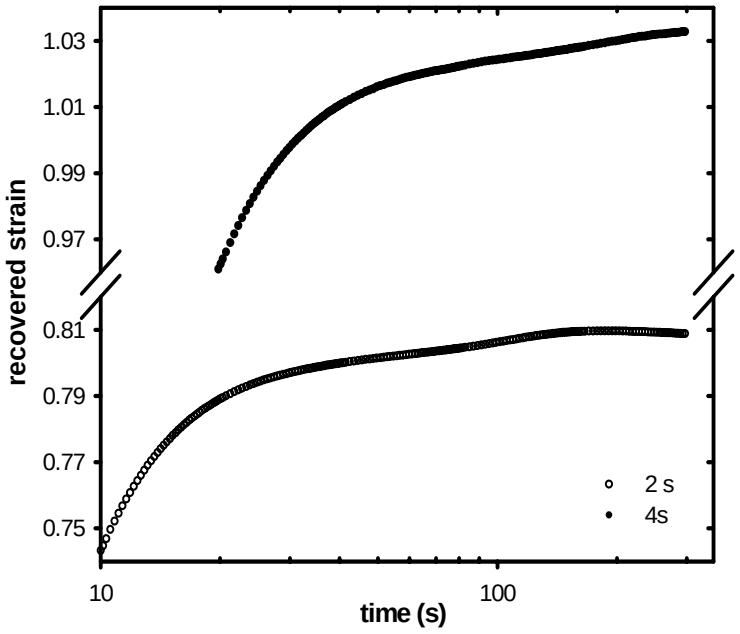

Fig.4.5 Recovery of blends after transient shear. (a) Recovery at various values of t_s with and without compatibilizer. Each pair (uncompatibilized and 0.2% compatibilized) is shifted upwards by a factor of 10 with respect to the previous t_s value. (b): Magnified views of the recovery curves at t_s = 2 s and t_s = 4 s. Note that the y-axis in (b) is linear.

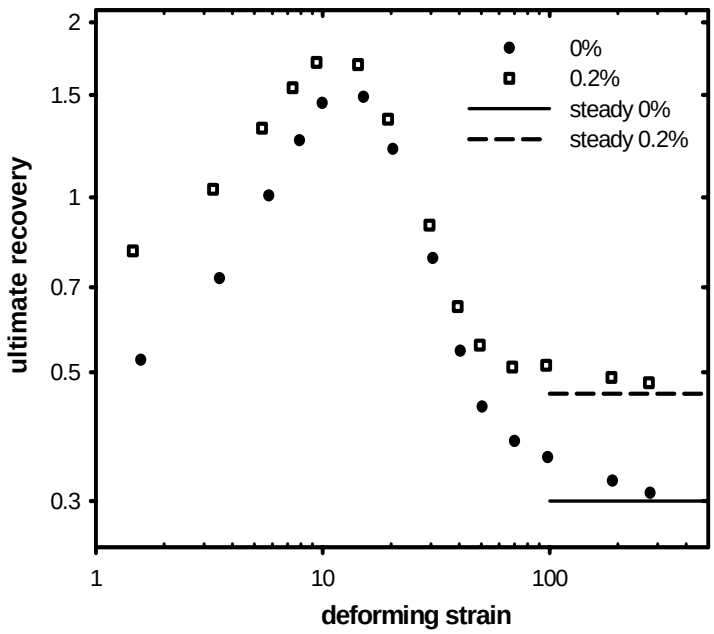

Fig.4.6 Recovery of blends presheared at 30 Pa for 2000 strain units, followed by 120 Pa for strains plotted on the x axis.

Fig.4.6 summarizes the results of the most important parameter of Fig.4.5: the ultimate recovery. Clearly, the trends are clear: that the compatibilizer increases the ultimate recovery in transient deformations at all values of t_s, with the largest effects being at small t_s.

4.3 DISCUSSION AND POSSIBLE MECHANISMS

4.3.1 Uncompatibilized Blends

The theory of recovery of uncompatibilized blends from steady shearing was discussed in the previous chapter. Briefly, recovery is driven by the deformation and orientation of drops along the flow direction. Under steady shear conditions, the ultimate recovery and the dimensionless retardation time are both proportional to the Ca prior to recovery. Both these quantities also have additional dependences on viscosity ratio and volume fraction of the drops.

The recovery upon transient shearing is more complex since the deformations can be much larger. As discussed by Vinckier *et al.* [38], the data of Fig. 4.6 can be divided into three regions. On the left of the maximum (deforming strain, $\gamma_s < 10$), the applied stress deforms the drops, and strain recovery is completed when deformed droplets retract, hence, increasing deformation increases the ultimate recovery and the retardation time. On the right of the maximum ($10 < \gamma_s < 60$) on the other hand, the deformation creates very highly elongated cylinders, and recovery is completed when these cylinders break by capillary instabilities. In this region, increasing strain causes cylinders with smaller diameter, thus reducing the time for capillary instabilities, and hence reducing the ultimate recovery and the retardation time. Finally, at very high shearing times ($\gamma_s > 100$), cylinder breakup is completed during the shearing itself. Thus when shearing is stopped, the morphology consists of drops that are smaller, and hence less deformed, than the original drops. Recovery involves retraction of these drops and since their size changes very slowly with strain, the ultimate recovery is nearly independent of strain.

4.3.2 Compatibilized Blends

As we are considering the compatibilizer (copolymer with blends) to act only as a surfactant that reduces the equilibrium interfacial tension between the phases, the coupling between flow, interfacial deformation, and the compatibilizer concentration must be considered: As discussed in Section 1.3.2, flow can induce gradients in surfactant concentration on the interface. To summarize briefly, in steady flow, the tips of the drops have a higher concentration of compatibilizer, and hence a lower interfacial tension. This lowers the capillary pressure of the tips, but also induces a Marangoni stress.

The non-uniform interfacial tension can affect recovery directly and indirectly. The indirect effect is that the initial deformation of compatibilized drops, i.e. the deformation at the instant recovery begins, is expected to be different from uncompatibilized ones. The direct effect is that the stresses driving retraction of the drops (and hence blend recovery) are modified by compatibilizer. For example, as the drop retracts, the average compatibilizer concentration on its surface increases, thus reducing the average interfacial tension, and hence the capillary pressure driving recovery. This is expected to slow the recovery of compatibilized blends. In contrast, the Marangoni stress is an additional factor driving the recovery of compatibilized drops, which is expected to increase the ultimate recovery and reduce the retardation time. The effects of compatibilizer on the recovery process are quite complex: compatibilizers can increase or decrease steady state deformation, and accelerate or retard drop dynamics depending on whether marangoni stresses or capillary pressure gradients dominate. Due to the high volume fraction of drops, the blends studied scatter light strongly and *in situ* visualization is difficult to conduct. In

the absence of even qualitative information from flow visualization, we are unable to speculate on the exact mechanism by which compatibilizer increases the strain recovered and the retardation time.

However, the slow retardation process of Fig. 4.5b may be explained on the basis of past simulations. Velankar *et al*. [72] studied the relaxation of single drops with surfactant after cessation of steady shear. They found a slow relaxation process developing at small compatibilizer content and attributed it to the interfacial tension gradients developed during drop deformation. Briefly, it was found that at some stage during drop retraction, the capillary pressure difference during retraction approached nearly zero causing slow subsequent relaxation. A similar mechanism may explain Fig. 4.5b.

5.0 CONCLUSION AND FUTURE WORK

In this thesis, we studied the blends recovery by rheological measurements, which provided qualitative results for the understanding of different conditions (drop fraction, viscosity ratio, compatibilizers effects, shear history) on the blends strain recovery. In the future, tests with different measurements methods should be carried out to study more about the blends dynamics under different conditions.

5.1 COMPATIBILIZER EFFECTS ON THE STEADY SHEAR VISCOSITY OF BLENDS

In all of this research, only blends with droplet-matrix morphologies were studied, however for droplets fraction close to 0.5, blends tend to have a disordered two phase morphology. It is not clear how compatibilizer affects rheological properties under these conditions.

In the tests conducted in this research, the shear viscosity of blends was recorded to compare the compatibilizer effects on the steady shear viscosity of blends. The results are shown in Fig. 5.1. It shows for the 50% blends, the viscosity of blends increases very much with the compatibilizer (wt %) increases while the effects of compatibilizer are much less for all other blends (10%, 20%, 30%). It is speculated this is due to the difference of morphology between

50% blends and all other blends. This is very interesting phenomenon, and will be a good starting point for further investigations.

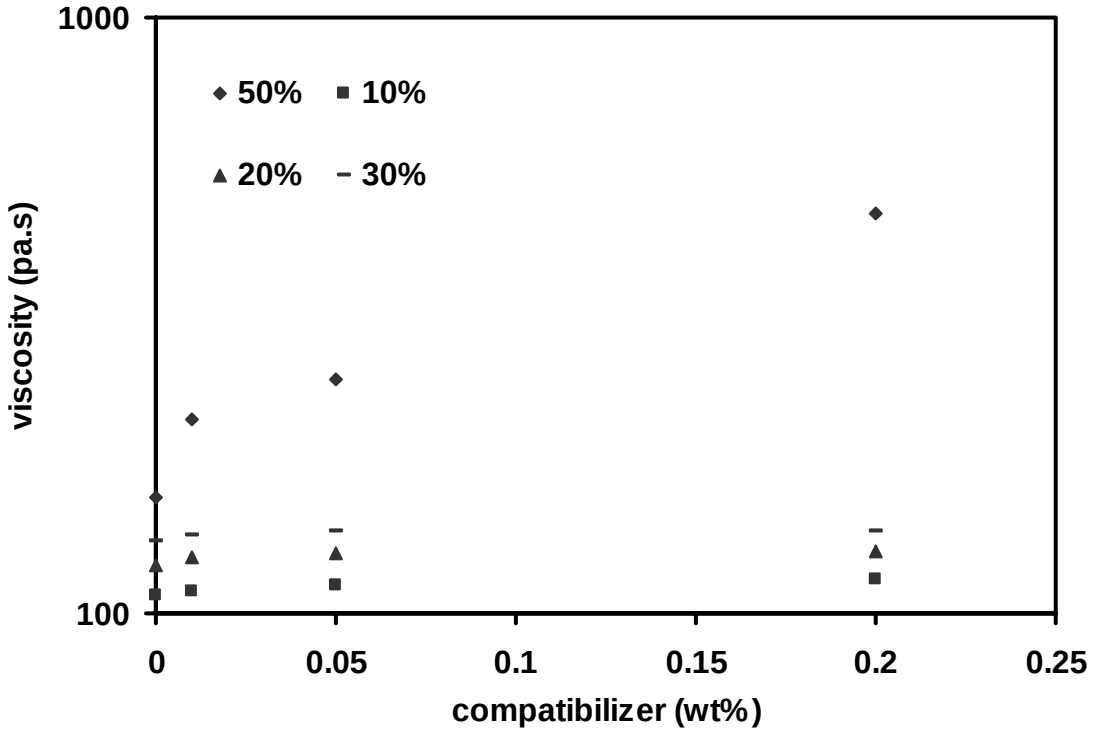

Fig 5.1 Compatibilizer effects on the steady shear viscosity of blend (10%, 20%, 30% and 50% PIB)

5.2 DROP SIZES AND SHAPES

In this thesis, by rheological measurements provided qualitative results for the understanding of blends strain recovery under different conditions. However, a more detailed understanding requires direct visualization of the morphology. In the future, the use of other techniques such as direct *in situ* visualization to study the quantitative change of drop sizes and shapes in the blends

is recommended. In particular, direct visualization may at least permit comments on whether compatibilized drops are more or less deformed than uncompatibilized ones.

5.3 FLUORESCENT COMPATIBILIZER

Flow visualization can address the issue of whether drops are more deformed or not. However the key issue of this study is that the compatibilizer is not uniformly distributed on the interface. This may be studied by fluorescently labeled compatibilizers [73].

In the future, the use of a method of fluorescent compatibilizer is recommended to visualize the compatibilizer concentration gradients on the drop surface.

APPENDIX

PROCEDURE FOR OBTAINING THE RELAXATION TIME OF THE SHOULDER IN G′

The relaxation time spectra of blends have been analyzed previously to find the relaxation time τ_d corresponding to the shoulder in G′ of the blends [23, 28]. There are however some numerical difficulties in obtaining a nearly continuous (typically 50 points per decade) relaxation spectrum of a material from its dynamic moduli. A procedure to obtain the relaxation time of the shoulder accurately without calculating the continuous relaxation spectra was devised previously [52]. It can find the relaxation time, τ_1 of model blends from their discrete relaxation spectra using a sum of very few Maxwell modes. It was applied in this research to obtain τ_1 of uncompatibilized blends with 10% drops. We illustrate the procedure here.

Fig. A-1 shows that the moduli and dynamic viscosity of the blends at high frequency are roughly equal to those expected for the components i.e. the high frequency moduli and dynamic viscosity are dominated by the component contributions. This suggests that subtracting the contribution of the components will accentuate the shoulder in G′ and reduce the number of Maxwell modes required for fitting. Accordingly, $\log(G'_{interface}) = \log(G'_{measured} - G'_{components})$ was fitted to

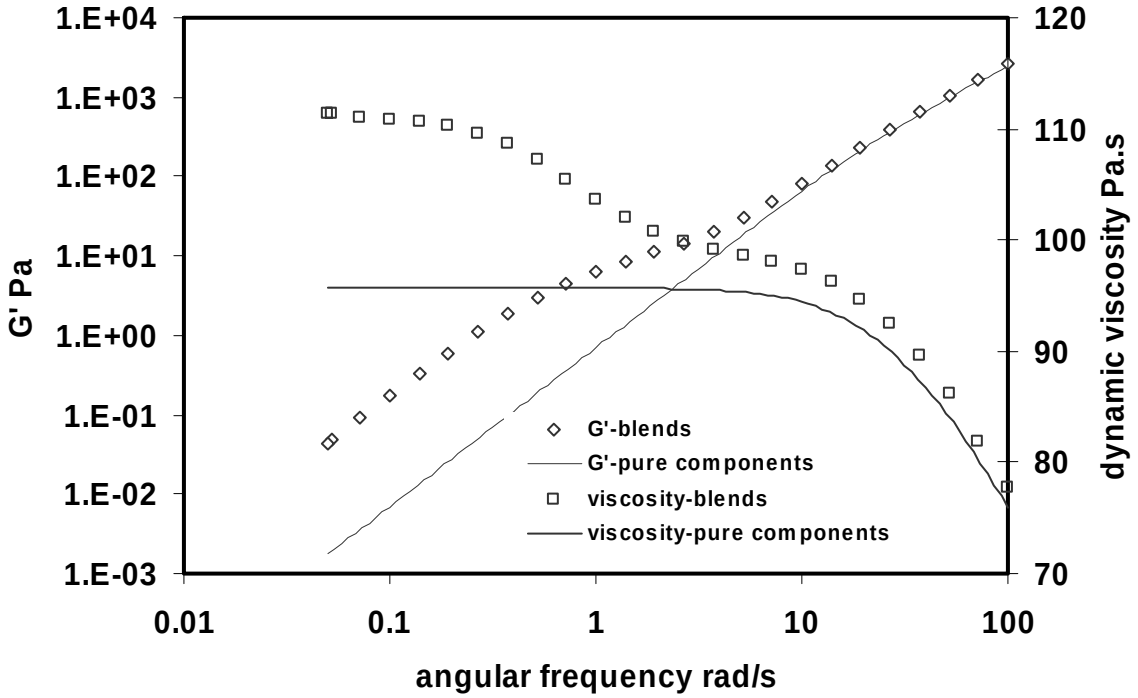

Fig. A-1 Typical dynamic moduli and dynamic viscosity data for blends. These data refer to uncompatibilized blends (10% PIB, 90%PDMS, and viscosity ratio is 1.1) after shearing at 120 Pa till steady state was reached. Solid lines were calculated using the Palierne model without interfacial tension, and thus represent the contribution expected from the pure components.

$$\log[G'(\omega)] = \log\left\{\sum_{k=1}^{n} \frac{\omega^2 \exp(a_k + 2t_k)}{1 + \omega^2 \exp(2t_k)}\right\} \qquad \text{(A-1)}$$

as suggested by Sector [74]. Here $\exp(t_k)$ and $\exp(a_k)$ are the relaxation time and the infinite-frequency modulus of the k^{th} Maxwell mode repectively. Fits were performed using the gnufit utility in 'gnuplot' software, and log of the moduli were used for fitting so that the relative error would be spread uniformly across the entire frequency range.

The component contribution was assumed to be given by the Dickie model [75] (or equivalently, by the Palierne model [27] with interfacial tension set to zero). Typical results of $G'_{interface} = G'_{measured} - G'(\sigma=0)$, and corresponding fits of Eq.A-1. are shown in Fig.A-2. Errors in estimating τ_1 caused by errors in estimating the component contribution are quite small since the component contribution is negligible at low frequencies. Fig. A-2 also shows that the magnitude of the corresponding η^*

$$|\eta^*(\omega)| = \frac{|G^*(\omega)|}{\omega} = \frac{\sqrt{G'(\omega)^2 + G''(\omega)^2}}{\omega} \qquad \text{(A-2)}$$

predicted by the a_k and t_k obtained from the fits agree well with

$$|\eta^*_{interface}| = |\eta^*_{measured} - \eta^*(\alpha=0)| \qquad \text{(A-3)}$$

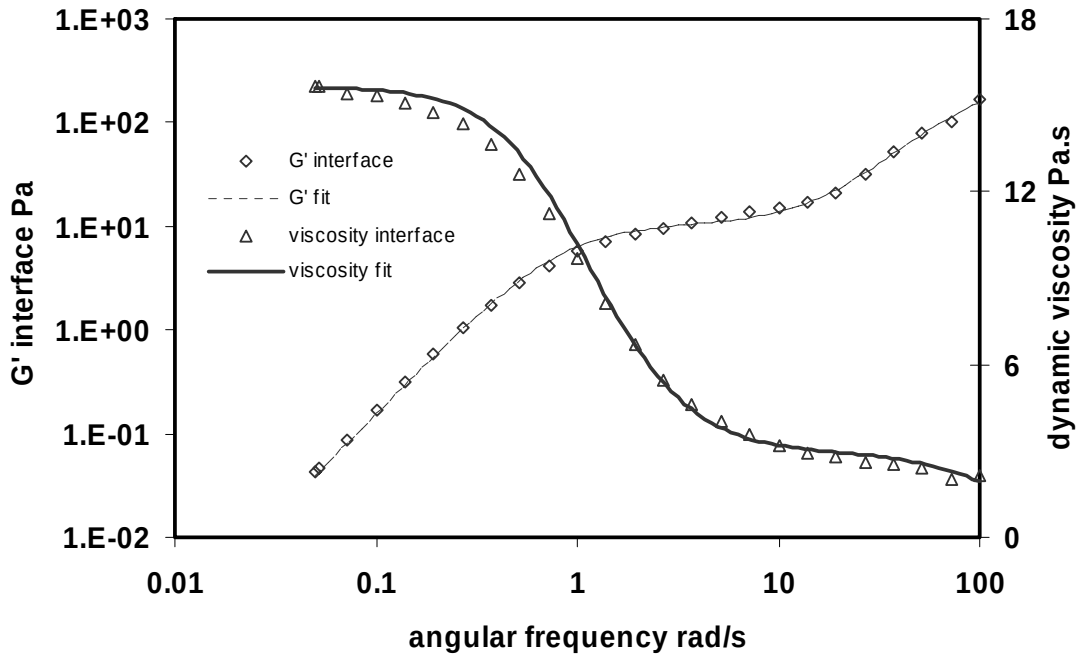

Fig.A-2. A typical example of fits to $G'_{interface}$ and $|\eta'_{interface}|$. $G'_{interface}=G'_{measured}-G'(\sigma=0)$ and $|\eta'_{interface}|=|\eta'_{measured}-\eta'(\sigma=0)|$. Symbols are typical examples of $G'_{interface}$ and $\eta^*_{interface}$ (same data as Fig. A-1). The lines are fitted using the results from Eq.A-1 with n as 2.

BIBLIOGRAPHY

1. Utracki, L.A., *Polymer Alloys and Blends*. 1989, Munich: Hanser Publishers.

2. Castro, M. and Christian.C.Frederic.P., *Experimental and theoretical description of low frequency viscoelastic behaviour in immiscible polymer blends.* Polymer, 2004. 45: p. 4095-4104.

3. Taylor, G.I., *The viscosity of a fluid containing small drops of another fluid.* Proc. Roy. Soc. London Ser., 1932. A(138): p. 41-48.

4. Taylor, G.I., *The formation of emulsions in definable fields of flow.* Proc. R. Soc. London Ser., 1934. A(146): p. 501-523.

5. Stone, H.A., *Dynamics of drop deformation and breakup in viscous fluids.* Annu. Rev. Fluid Mech., 1994. 26: p. 65-102.

6. Rayleigh, L., *On the instability of jets.* Proc. Math. Soc. Lond., 1879. 10: p. 4.

7. Rayleigh, L., *On the capillary phenomena of jets.* Proc. Lond. Math. Soc., 1879. 10: p. 71.

8. Mikami, T., Cox, R.G., Mason, S.G., *Breakup of extending liquid threads.* Int. J. Multiphase Flow, 1975. 2: p. 113-138.

9. Grace, H.P., *Dispersion phenomena in high viscosity immiscible fluid systems and application of static mixers as dispersion devices in such systems.* Chem. Eng. Commun., 1971. 14(225-277).

10. Tomotika, S., *On the instability of a cylindrical thread of a viscous liquid surrounded by another viscous fluid.* Proc. R. Soc. London Ser., 1935. A(150): p. 322-337.

11. Tomotika, S., *Breaking up of a drop of viscous liquid immersed in another viscous fluid which is extending at a uniform rate.* Proc. R. Soc. London Ser., 1936. A(153): p. 302-318.

12. Khakhar, D., Ottino, J., *Breakup of liquid threads in linear flows.* Int. J. Multiphase Flow, 1987. 13: p. 71-86.

13. Janssen, J.M.H., Meijer, H. E. H., *Droplet Breakup Mechanisms - Stepwise Equilibrium Versus Transient Dispersion.* Journal of Rheology, 1993. 37(4): p. 597-608.

14. Stone, H.A., Bentley, B.J., Leal, L.G., *An experimental study of transient effects in the breakup of viscous drops.* J. Fluid Mech., 1986. 198: p. 339-427.

15. Stone, H.A., Leal, L.G., *Relaxation and breakup of an initially extended drop in an otherwise quiescent fluid.* J. Fluid Mech., 1989. 198: p. 399-427.

16. Son, Y., Martys, N. S., *suppression of capillary instability of a polymeric thread via parallel plate confinement.* Macromolecules, 2003. 36: p. 5825.

17. Pal, R., *Rheology of polymer-thickened emulslons.* J. Rheol, 1992. 36(7): p. 1245.

18. Choi, S.J., Schowalter, W.R., *Rheological properties of nondilute suspensions of deformable particles.* Phys. Fluids, 1975. 18: p. 420-27.

19. Vinckier, I., Mewis, J., Moldenaers, P., *Rheology of semi-dilute emulsions: viscosity effects caused by the interfacial tension.* Colloids and Surfaces A, 1999. 150(217-228).

20. Graebling, F.D., Muller R., *Viscoelastic properties of polydimethylsiloxane-polyoxyethylene blends in the melt. Emulsion model.* J. Rheol., 1989. 33: p. 1283-1291.

21. Graebling, F.D., Muller,R., Palierne,J.F., *Linear viscoelastic behavior of some incompatible polymer blends in the melt. Interpretation of data with a model of emulsion of viscoelastic liquids.* Macromolecules, 1993. 26: p. 320-329.

22. Graebling, F.D., Muller R. , Palierne J.F., *Linear viscoelasticity of incompatible polymer blends in the melt in relation with interfacial properties.* J. Phys., 1993. IV(3): p. 1525-1534.

23. Gramespacher, H., Meissner, J., *Interfacial tension between polymer melts measured by shear oscillations of their blends.* J. Rheol., 1992. 36: p. 1127-1141.

24. Takahashi, Y., H. Suzuki, Y. Nakagawa. I. Noda, *Viscoelastic properties of polystyrene-poly(vinyl methylether) blends in oscillatory and steady shear flows near the phase separation temperature.* Polym. Int., 1994. 34: p. 327-332.

25. Friedrich, C., Gleinser, W., Korat, E., Maiser, E., Weese, J., *Comparison of sphere-size distributions obtained from rheology and transmission electron microscopy in PMMA/PS blends.* J. Rheol., 1995. 36: p. 1411-1425.

26. Oldroyd, J., *The elastic and viscous properties of emulsions and suspensions.* Proc. Roy. Soc. Lond. Ser. A, 1953. 218: p. 122-132.

27. Palierne, J., *Linear rheology of viscoelastic emulsions with interfacial tension.* Rheol. Acta, 1990. 29: p. 204-214.

28. Vinckier, I., Moldenaers, P., Mewis, J., *Relationship between rheology and morphology of model blends in steady shear flow.* J. Rheol, 1996. 40(4): p. 613-631.

29. Grizzuti, N., Bifulco, O., *Effects of coalescence and breakup on the steady state morphology of an immiscible polymer blend in shear flow.* Rheol. Acta, 1997. 36(4): p. 406-415.

30. Vinckier, I., Mewis, J., Moldenaers, P., *Stress relaxation as a microstructural probe for immiscible polymer blends.* Rheol. Acta, 1997. 36: p. 512-523.

31. Yamane, H., Takahashi, M., Hayashi, R., Okamoto, K., Kashihara, H., Masuda, T., *Observation of deformation and recovery of poly(isobutylene) droplet in a poly(isobutylene) / poly(dimethyl siloxane) blend after application of step shear strain.* J. Rheol., 1998. 42: p. 567-80.

32. Okamoto, K., Tamura, R., Ishikawa, M., *Observation of coalescence of two polyisobutylene droplets in polydimethylsiloxane under large step shear strain.* Journal of the Society of Rheology Japan, 2002. 30(1): p. 45-48.

33. Guido, S., Villone, M., *Measurement of interfacial tension by drop retraction analysis.* J. Colloid Int. Sci., 1999. 209: p. 247-50.

34. Jansseune, T., Vinckier, I., Moldenaers, P., Minale, M., Mewis, J., *Transient stresses in immiscible model polymer blends during start-up flows.* J. Non-Newtonian Fluid Mech., 2001. 99: p. 167-181.

35. Thornton, B.A., *The melt elasticity of polymer blends:polystyrene / poly(methyl methacrylate).* J. Appl. Polym. Sci., 1980(25): p. 653-663.

36. Gramespacher, H., Meissner, J., *Melt elongation and recovery of polymer blends, morphology, and influence of interfacial tension.* J. Rheol., 1997. 41: p. 27-44.

37. Vinckier, I., Moldenaers, P., Mewis, J., *Elastic recovery of immiscible blends Part 1. Analysis after steady state shear flow.* Rheol. Acta, 1999. 38: p. 65-72.

38. Vinckier, I., Moldenaers, P., Mewis, J., *Elastic recovery of immiscible blends Part 2. Transient flow histories.* Rheol. Acta, 1999. 38: p. 198-205.

39. Gramespacher, H., Meissner, J., *Reversal of recovery direction during creep recovery of polymer blends.* J. Rheol., 1995. 39: p. 151-60.

40. Gronski, W., Lauger, J., Laubner, C., *Structure development under shear flow during spinodal decomposition of a polymer blend observed by simultaneous measurement of*

small angle light scattering and rheological functions. Journal of Molecular Structure, 1996. 383(1-3): p. 23-30.

41. Di Lorenzio, M.L., Frigione, M., *Compatibilization criteria and procedures for binary blends: A review.* J. Polym. Eng, 1997. 17: p. 429-459.

42. Koning, C., Van Duin, M. Pagnoulle, C., Jerome, R., *Strategies for compatiblization of polymer blends.* Prog. Polym. Sci, 1998. 23: p. 707-757.

43. Van Puyvelde, P.V., S., Moldenaers, P., *Rheology and morphology of compatibilized polymer blends.* Curr. Opin. Colloid Interface Sci., 2001. 6: p. 457-463.

44. Sundararaj, U., Macosko, C.W., *Drop breakup and coalescence in polymer blends: The effects of concentration and compatibilization.* Macromolecules, 1995. 28: p. 2647-2657.

45. Macosko, C.W., Guegan, P., Khandpur, A.K., Nakayama, A., Marechal, P., Inoue, T., *Compatibilizers for melt blending: Premade block copolymers.* Macromolecules, 1996. 29: p. 5590-5598.

46. Milner , S.T., Xi, H., *How copolymers promote mixing of immiscible homopolymer.* J. Rheol, 1996. 40: p. 663-687.

47. Ramic, A.J., Stehlin, J.C., Hudson, S.D., Jamieson, A.M., Manas-Zloczower, I., *Influence of block copolymer on droplet breakup and coalescence in model immiscible polymer blends.* Macromolecules, 2000. 33: p. 371-374.

48. Riemann, R.E., Cantow, H.J., Friedrich, C., *Interpretation of a new interface governed relaxation process in compatibilized polymer blends.* Macromolecules, 1997. 30: p. 5476-5484.

49. Jacobs, U., Fahrlander, M., Winterhalter, J., *Analysis of Palierne's emulsion model in the case of viscoelastic interfacial properties.* J. Rheol., 1999. 43(6): p. 1495-1509.

50. Hu, Y.T., Pine, D.J., and Leal, L.G., *Drop deformation, breakup, and coalescence with compatibilizer.* Phys. Fluids, 2000. 12: p. 484-489.

51. Velankar, S., Van Puyvelde, P., Mewis, J., Moldenaers, P., *Effect of compatibilization on the breakup of polymeric drops in shear flow.* J. Rheol., 2001. 45(4): p. 1007-1019.

52. Velankar, S., Van Puyvelde, P., Mewis, J., Moldenaers, P., *Steady-shear rheological properties of model compatibilized blends.* J. Rheol., 2004. 48(4): p. 725-744.

53. De Bruijn, R.A., *Tip streaming drops in simple shear flows.* Chem. Eng. Sci., 1993. 48: p. 277-84.

54. Eggleton, C.D., Tse-Min Tsai., Stebe, K.J., *Tip streaming from a drop in the presence of surfactants.* Phy. Rev. Lett., 2001. 87: p. 4.

55. Kennedy, M.R., Pozrikidis, C., Skalak, R., *Motion and deformation of liquid drops and the rheology of filute emulsions in simple shear flow.* Comput. Fluids, 1994. 23: p. 251-278.

56. Loewenberg, M.H., E.J., *Numerical simulations of a concentrated emulsion in shear flow.* J. Fluid. Mech., 1996. 321: p. 395-419.

57. Charles, R., Pozrikidis, C., *Significance of the dispersed-phase viscosity on the simple shear flow of suspensions of two-dimensional liquid drops.* J. Fluid Mech, 1998. 365: p. 205-234.

58. Milliken, W.J., Stone, H.A., Leal, L.G., *The effect of surfactant on transient motion of Newtonian drops.* Phys. Fluids, 1993. 5: p. 69-79.

59. Pawar, Y., Stebe, K.J., *Marangoni effects on drop deformation in an extensional flow: The role of surfactant physical chemistry. I. Insoluble surfactants.* Phys. Fluids, 1996. 8: p. 1738-1751.

60. Li, X.F., Pozrikidis, C., *The effect of surfactants on drop deformation and on the rheology of dilute emulsions in Stokes flow.* J. Fluid Mech., 1997. 341: p. 165-194.

61. Eggleton, Y.P., Pawar, C.D., Stebe, K.J., *Insoluble surfactants on a drop in an extensional flow: a generation of the stagnated surface limit to deforming interfaces.* J. Fluid Mech., 1998. 385: p. 79-99.

62. Blawzdziewicz, J., Vlahovska, P., Loewenberg, M., *Rheology of a dilute emulsion of surfactant-covered spherical drops.* Physica A, 2000. 276(1-2): p. 50-85.

63. Riemann, R.E., Cantow, H.J., Friedrich, C., *Rheological investigation of form relaxation and interface relaxation processes in polymer blends.* Polym. Bull, 1996. 36: p. 637-643.

64. Van Hemelrijck, E., Van Puyvelde, P., Velankar, S., Macosko, C. W., Moldenaers, P., *Interfacial elasticity and coalescence suppression in compatibilized polymer blends.* J. Rheol., 2004. 48(1): p. 143-158.

65. Vinckier, I., Moldenaers, P., Mewis, J., *Transient rheological response and morphology evolution of immiscible polymer blends.* J. Rheol., 1997. 41(3): p. 705-718.

66. Jansseune, T., Mewis, J., Moldenaers, P., Minale, M., Maffettone, PL., *Rheology and rheological morphology determination in immiscible two-phase polymer model blends.* J. Non-Newtonian Fluid Mech., 2000. 93: p. 153-65.

67. Wagner, M., Wolf, B. A., *Interfacial-tension between poly(isobutylene) and poly(dimethylsiloxane) - Influence of chain-Length, temperature, and solvents.* Macromolecules, 1993. 26(24): p. 6498-6502.

68. Sigillo, I., Santo, L., Guido, S., Grizzuti, N., *Comparative measurements of interfacial tension in a model polymer blend.* Polym. Engng. Sci., 1997. 37: p. 1540-1549.

69. Velankar, S., et al., *Effect of compatibilization on the breakup of polymeric drops in shear flow.* J. Rheol., 2001. 45(4): p. 1007-1019.

70. Yang, H., Zhang, H., Moldenaers, P., Mewis, J., *Rheo-optical investigation of immiscible polymer blends.* Polymer, 1998. 39: p. 5731-37.

71. Maffettone, P.L., Minale, M., *Equation of change for ellipsoidal drops in viscous flow.* J. Non-Newtonian Fluid Mech., 1998. 78(2-3): p. 227-241.

72. Velankar, S., Zhou, H., Jeon, H. K., Macosko, C. W., *CFD evaluation of drop retraction methods for the measurement of interfacial tension of surfactant-laden drops.* Journal of Colloid and Interface Science, 2004. 272(1): p. 172-185.

73. Jeon, H.K., Feist, B. J., Koh, S. B., Chang, K., Macosko, C. W., Dion, R. P., *Reactively formed block and graft copolymers as compatibilizers for polyamide 66/PS blends.* Polymer, 2004. 45(1): p. 197-206.

74. Secor, R.B., *Appendix 3A*, in *Rheology principles, measurements, and applications*, C.W. Macosko, Editor. 1993, VCH Publishers, Inc: New York.

75. Dickie, R.A., *Heterogenerous polymer-polymer composites. I. Theory of viscoelastic properties and equivalent mechanical models.* J. Appl. Polym. Sci., 1973. 17: p. 45-63.